sciendo
Austrian Journal of Earth Sciences | Vienna | 2025 | Volume 118 | 95–114 | DOI: 10.17738/ajes.2025.0005

Zircon ages and differentiation trend of Ordovician granitoids from the southeastern Ötztal Nappe (Texelgruppe, South Tyrol, Italy): ridge subduction at the margin of Gondwana?

Linus Klug[1]*, Nikolaus Froitzheim[1], Frank Tomaschek[1]

[1)] Institute of Geosciences, University of Bonn, Meckenheimer Allee 169, 53115 Bonn, Germany
[*)] Corresponding author: Linus Klug, email: klug@uni-bonn.de

Keywords: Eastern Alps, Austroalpine basement, Gondwana, Geochronology

Abstract

The Austroalpine Ötztal Nappe and the adjacent Marlengo Slice comprise pre-Variscan basement of Neoproterozoic to Early Paleozoic metasedimentary rocks intruded by Ordovician granitoids now present as orthogneisses. LA-ICPMS U-Pb zircon dating complemented by whole-rock geochemistry on orthogneisses from the Texelgruppe, the southeastern part of the Ötztal Nappe, and the Marlengo Slice yields an Ordovician differentiation trend from ~470 Ma to ~447 Ma, evolving from arc to collision and finally post-orogenic granitoid signature. We interpret this as an expression of a contemporaneous mid ocean ridge subduction under the active margin of Northeastern Gondwana. Abundant zircon cores exhibit an age distribution inherited from the sedimentary melt source of the orthogneisses with S-type geochemistry and record influence by the Northeast-Africa-Arabia Zircon Province and the Cadomian magmatic arc.

1. Introduction

The Variscan basement units of the Alps represent important elements of the European Variscides. They are crucial for the tectonic and paleogeographic reconstruction of the Variscan Orogeny and of Early Paleozoic plate tectonics leading up to it. On one hand, these units are better exposed than many extra-Alpine parts of the Variscan orogen. On the other hand, however, their reconstruction is complicated by strong Alpine tectonic and metamorphic overprint.

The Early Paleozoic tectonic framework of the Variscan basement of the Alps is under debate. Different interpretations exist with respect to the Austroalpine Units, generally interpreted as belonging to the northern margin of Gondwana during the Early Paleozoic (e.g. Frisch and Neubauer, 1989; von Raumer, 1998; Schulz et al., 2008; von Raumer and Stampfli, 2008; Spiess et al., 2010; Stampfli et al., 2013; von Raumer et al., 2013; Zurbriggen, 2015, 2017; Stephan et al., 2019; Siegesmund et al., 2021, 2023; Neubauer et al., 2022; Finger and Riegler, 2023). The Paleozoic setting is preceded by the Archean-Proterozoic crustal mobilization event (ca. 2.5 Ga), the Proterozoic mantle mobilization event (ca. 1 Ga) and the Neoproterozoic breakup of the Gondwana margin (ca. 650–600 Ma) (von Raumer et al., 2013). For the Ediacaran to Early Paleozoic, all models have in common that the Austroalpine and its tectonic subunits (e.g. Ötztal Nappe, Marlengo Slice) are positioned on the northern margin of Gondwana. The margin geometry, the geodynamic processes, and the positions of different units along the margin are under debate. A consensus exists that part of the northern Gondwana margin is today represented by northern Africa and Arabia and that the Austroalpine lay further to the east along this margin than most other central European Paleozoic units, which means that the Austroalpine was in proximity to northeast Africa and Arabia (e.g. Stephan et al., 2019). The name of the ocean north of the Gondwana margin varies between Celtic Ocean (Zurbriggen, 2017, 2020), Iapetus Ocean (e.g. Oriolo et al., 2021), Proto-Rheic Ocean (e.g. Finger and Riegler, 2023), Proto-Tethys Ocean (e.g. Siegesmund et al., 2023), and Qaidam Ocean (e.g. Neubauer et al., 2022). The exact timing, position and tectonic framework of the Cadomian and Cenerian orogenies is unclear. The Cadomian orogeny is mostly seen as a Late Ediacaran to Cambrian, Andean-style accretionary orogeny on an active continental margin (e.g. Siegesmund et al., 2023; Finger and Riegler, 2023). An associated arc-related magmatic flare-up at ca. 570–530 Ma is also reported in the Austroalpine and other basement units of the Alps (Siegesmund et al., 2021, 2023, and references therein). In the Ötztal Nappe, no Cadomian protolith ages have been found yet (e.g. Neubauer et al., 2022).

The tectonic setting of Late Cambrian to Ordovician (Cenerian) processes is either seen as a change from Andean-type to Alaskan-type subduction (e.g. Zurbriggen, 2015, 2017), a passive margin with rifting (e.g. Stephan et al., 2019), the eastward propagation of the Rheic-Ocean opening as a back-arc basin into a continental arc (e.g. Siegesmund et al., 2023), rifting-related terrane separation in an angled margin geometry (e.g. Stampfli et al., 2013; Neubauer et al., 2022), or a hyper-extended margin to the West giving way to an Alaskan-type coastal orogen to the East (Finger and Riegler, 2023).

This study provides new constraints for the Paleozoic setting of the Austroalpine basement, using geochronological and geochemical data from orthogneisses of the Ötztal Nappe (Texel Complex) and the Marlengo Slice located in the Texelgruppe in South Tyrol, Italy (Fig. 1). We show that these orthogneisses are derived from Ordovician granitoids which intruded over a time span of at least ~23 Ma from Middle (~470 Ma) to Late Ordovician (~447 Ma). We use U-Pb geochronology of magmatic zircon domains and inherited cores and whole-rock geochemistry to constrain the evolving tectonic setting of Ordovician magmatism in the Austroalpine.

2. Regional geology

The Texelgruppe is the part of the Ötztal Alps between the main drainage divide (Austrian-Italian border) to the north, the Passeier Valley to the east, the Meran basin and Vinschgau Valley to the South, and the Schnals Valley to the West. The area belongs to the Lower Central Austroalpine basement (Janák et al., 2004). The Texelgruppe is formed by metamorphic rocks recording a long history of tectonic, magmatic and metamorphic processes, which includes (1) Late Proterozoic to Paleozoic sedimentation and magmatism on the northern margin of Gondwana with sources in the Gondwana mainland, supplying Proterozoic to Archean zircon grains; (2) Variscan metamorphism and deformation; (3) Permo-Mesozoic crustal thinning; (4) early Eo-Alpine thrust emplacement of the Schneeberg Complex; (5) Eoalpine high-pressure metamorphism and deformation; (6) thrusting along the Vinschgau Shear Zone and exhumation of high-pressure rocks; (7) Tertiary faulting related to the Periadriatic fault system (Bargossi et al., 2010; Gregnanin and Sassi, 1969; Habler et al., 2006, 2009; Klug and Froitzheim, 2021; Miladinova et al., 2022; Montemagni et al., 2023; Pomella et al., 2012, 2016; Schmid and Haas, 1989; Sölva et al., 2001; Tropper et al., 2023; Viola et al., 2001; Zanchetta et al., 2013; Zantedeschi, 1991). Structurally it can be subdivided into the main tectonic units of the Ötztal Nappe (Texel Complex), the Marlengo Slice, and small parts of the Campo Nappe (Fig. 2) (Bargossi et al., 2010; Klug and Froitzheim, 2021). These are all Austroalpine units. The southwestern-most Texelgruppe near Meran is part of the Southalpine (Fig 2). The Marlengo Slice is separated from the Ötztal Nappe and the Campo Nappe by the Forst Fault (Bargossi et al., 2010). The Thurnstein Mylonites are cut off by the Forst Fault and separate the Ötztal Nappe from the Campo Nappe. The Forst Fault is, together with the Passeier Fault, part of the Giudicarie Fault System (Viola et al., 2001; Pomella et al., 2012). The Thurnstein Mylonites are assumed to be the eastern continuation of the Vinschgau Shear Zone (Pomella et al., 2016). The latter is a wide, Eoalpine shear zone becoming increasingly ductile from west to east (Schmid and Haas, 1989; Montemagni et al., 2023). It separates the Ötztal Nappe from the Campo Nappe. The Texel Complex is the south-eastern part of the Ötztal Nappe, separated from the main body of the nappe by the Schneeberg Complex, a unit of metasediments characterized by the absence of Variscan metamorphism. Where the Schneeberg Complex ends towards southwest, the Texel Complex is connected with the main body of the Ötztal Nappe (Ötztal Complex s. str.) (Klug and Froitzheim, 2021). This is evident by the continuous NW-SE trending Eoalpine metamorphic gradient (Klug and Froitzheim, 2021; Raso et al., 2025). The Ötztal Complex s. str. is the main part of the Ötztal Nappe without the Texel Complex and the Schneeberg Complex.

In the Texel Complex, multiple metamorphic and deformation phases trace a re-subduction of Variscan eclogite-bearing continental crust during the Eoalpine orogeny (Habler et al., 2006; Zanchetta et al., 2013; Miladinova et al., 2021). The spatial configuration of Eoalpine and Variscan metamorphism in basement units and their proposed sedimentary cover of pre- and post-Variscan age supports the lower-plate position (with respect to Eoalpine subduction) of the Texel Complex. It represents the most deeply subducted, high-pressure part of the Eoalpine Ötztal Nappe (Klug and Froitzheim, 2021). The Ötztal Nappe was exhumed, still during Late Cretaceous, between the Vinschgau Shear Zone thrust at its base and the Steinach Normal Fault at its top (Klug and Froitzheim, 2021; Montemagni et al., 2023).

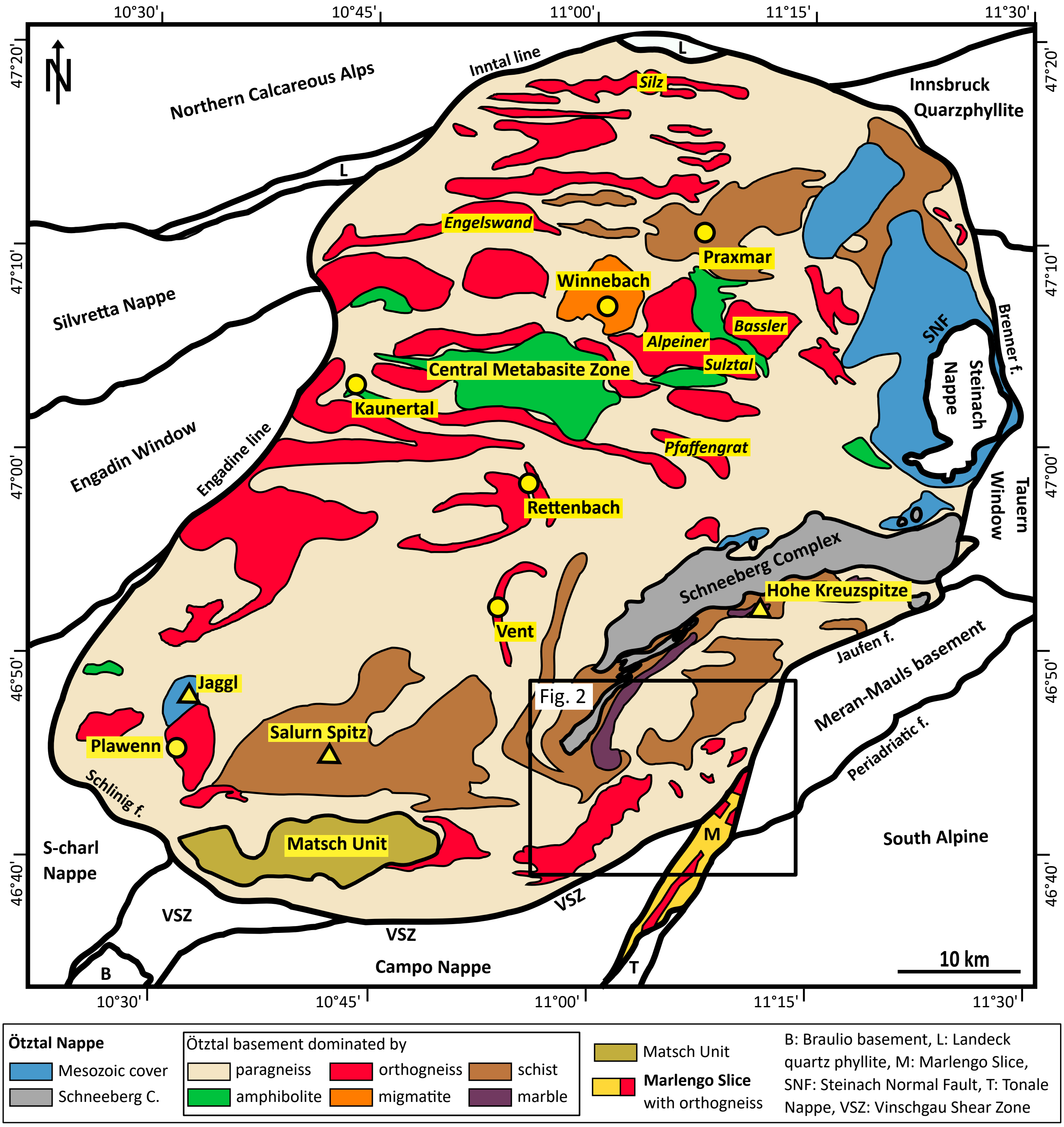

Figure 1: Geological overview map of the Ötztal Nappe and surroundings. Mod. after Brandner (1980), GeoSphere Austria (2024), Hauser (1992), Hammer (1923, 1929), Institut für Geologie, Universität Bern and Bundesamt für Wasser und Geologie (2005), ISPRA (1925, 1951, 1957, 1970, 2010, 2023), Klug and Froitzheim (2021), Kreuss (2011, 2012), Moser (2016a, b), Pavlik and Moser (2018), Rockenschaub and Nowotny (2009, 2011), Schindlmayr (1999).

The Ötztal Nappe consists of Variscan basement with its Mesozoic cover sediments. The Schneeberg Complex was thrust upon the deeper parts of the nappe before the peak of Eoalpine metamorphism in the Late Cretaceous (Klug and Froitzheim, 2021). The Variscan basement can be further subdivided into Palaeozoic metasedimentary units (Laas Unit, Schneeberg Frame Zone) and a presumably older basement. This older basement makes up most of the Ötztal Nappe and contains large bodies of orthogneiss. In addition to the orthogneisses, it consists of paragneiss, schist, quartzite, amphibolite, and eclogite, and is crosscut by Oligocene basic to intermediate dykes (Bargossi et al., 2010).

The Matsch Unit in the southwest part of the Ötztal Nappe consists of rocks typical for the Campo Nappe but lies in a hanging-wall position with respect to the

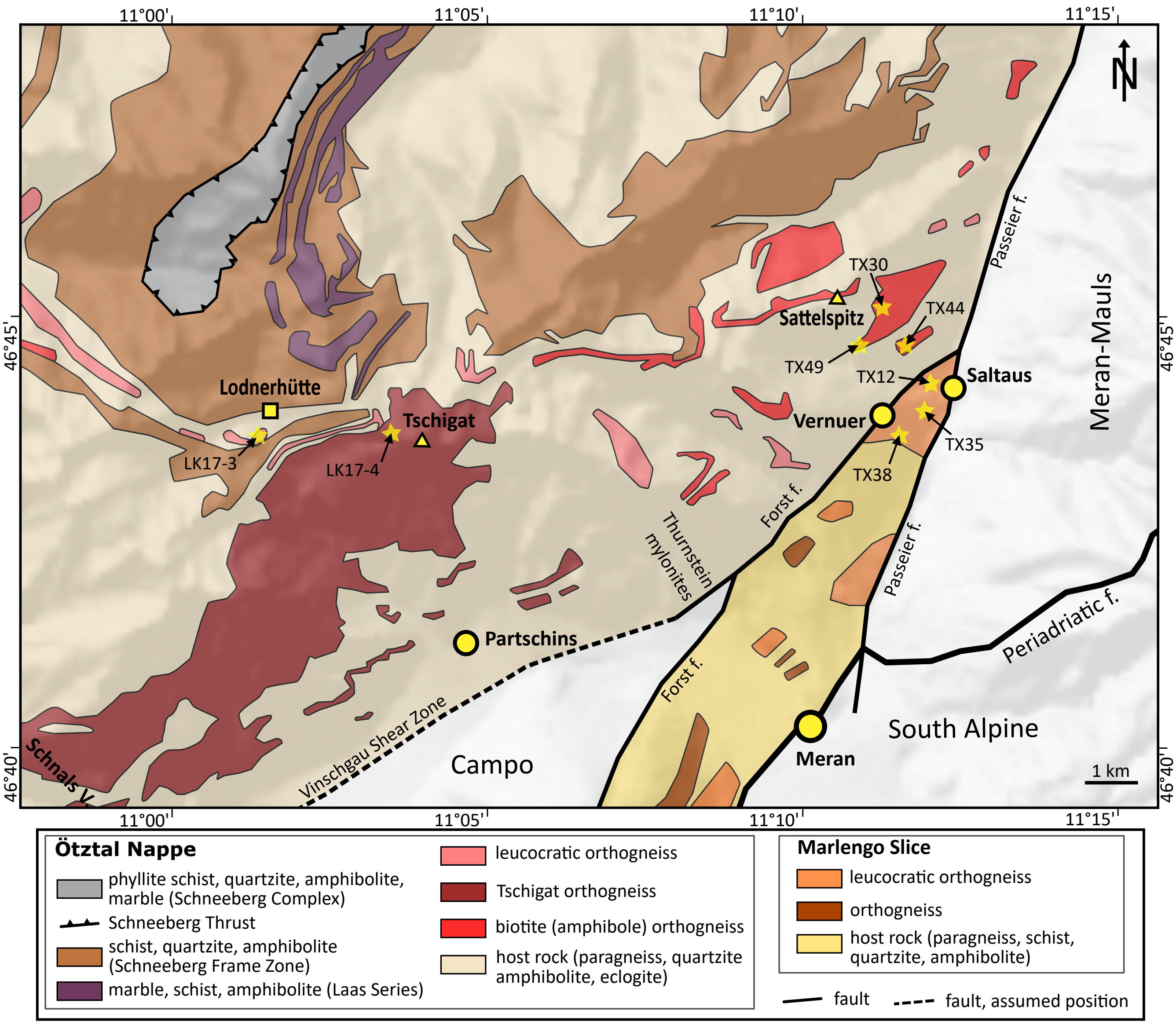

Figure 2: Map of the study area with sample locations. Mod. after ISPRA (1957, 1970, 2010), Kreuss (2012), Klug and Froitzheim (2021).

Vinschgau Shear Zone, in contrast to the Campo Nappe, which lies in the footwall of this shear zone (Habler et al., 2009). The Matsch Unit contains Permian pegmatites and exhibits upper-greenschist-facies Cretaceous metamorphism (Habler et al., 2009). There is no contrast in Eoalpine metamorphism between the Matsch Unit and the surrounding Ötztal Nappe (Schuster, 2003). This suggests an overthrust of the Matsch Unit over the Ötztal Complex s. str. before the peak of Eoalpine metamorphism and before the activity of the Vinschgau Shear Zone. This is similar to the early Eoalpine emplacement of the Schneeberg Complex along the Schneeberg Thrust (Klug and Froitzheim, 2021).

Bargossi et al. (2010) described no occurrences of pegmatites in the Ötztal Nappe on the geological map sheet Meran, while slightly north of this area (Hohe Kreuzspitze) Schneider (2013) described a pegmatite occurrence in the Texel Complex and dated it using U-Pb geochronology on cassiterite and columbite, which yielded Permian ages of 288.7 Ma and 274 Ma, respectively.

The Marlengo Slice represents a shallow part of the Lower Central Austroalpine nappe stack (Janak et al., 2004). It is juxtaposed to the Ötztal Nappe along a Tertiary fault, the Forst Fault (Bargossi et al., 2010). The southern end of the Marlengo Slice is not well constrained. On the geological map sheet Apiano (Avanzini et al., 2007) it is not mentioned. It wedges out between the Campo Nappe and the Tonale Nappe (Bargossi et al., 2010). The rock inventory of the Marlengo Slice differs from the Campo Nappe in that it lacks pegmatites and marbles. Moreover, the Marlengo Slice differs structurally from the surrounding units in the orientation of S2 foliation (Bargossi et al., 2010). It contains quartzitic gneiss, micaschist, quartzite, (leucocratic) orthogneiss, and amphibolite.

The northern end of the Marlengo Slice must lie north of the Saltaus Valley, a side valley of the Passeier Valley west of Saltaus, because leucocratic orthogneisses typical for the Marlengo Slice crop out southeast of the assumed continuation of the Forst Fault in the lower Saltaus Valley (Klug, 2016). The Forst Fault was active at the same time as the Passeier Fault and the Giudicarie Fault (Pomella et al., 2012). Pseudotachylites from the northern Forst Fault near Vernuer were dated at 17.3 Ma (Ar-Ar, Müller et al., 2001).

3. Early Paleozoic tectonics and magmatism of the Ötztal Nappe in the Austroalpine framework

The oldest rocks of the Ötztal Nappe are the paragneisses; they are also the most widespread ones. Detrital zircon ages hint to a late- to post-Cadomian, i.e. Cambrian deposition age (Siegesmund et al., 2021). The Central Metabasite Zone of the Ötztal Nappe comprises metamorphosed gabbros and basalts with MORB affinity (Mogessie et al., 1985, Miller and Thöni, 1995) emplaced during Early Cambrian (517 ±7 Ma; Konzett et al., 2005) in a back-arc setting (Siegesmund et al., 2021). Neubauer et al. (2022) correlated this zone with the Speik Complex in the eastern Austroalpine and interpreted it as an obducted ophiolite.

Late Cambrian to Ordovician protolith ages have been published for orthogneisses from the Ötztal Nappe. Gregnanin and Sassi (1969) were first to describe the Tschigat orthogneiss as of magmatic origin. Söllner and Hansen (1987) performed whole-rock Rb/Sr and zircon-fraction-leaching U-Pb measurements on rocks from the Winnebach area, the Vent area (Venter Schlinge) and the Rettenbachtal area (Mittelberg Schlinge). However, the ages are compromised by methodological limitations, i.e., separation of growth phases in zircons and opening of the Rb/Sr system. Zantedeschi (1991) performed whole-rock Rb-Sr dating on rock samples of the Tschigat orthogneiss. This did not yield an isochron but a rough alignment at about 450 Ma. Bernhard et al. (1996) produced magmatic protolith ages of 485 Ma for amphibole-bearing orthogneisses from the Kaunertal by Pb-Pb single zircon evaporation and Sm-Nd titanite dating. Klötzli-Chowanetz et al. (1997) determined a migmatisation age of 490 ±9 Ma for the Winnebach Migmatite by U-Pb multi-grain analysis. Klötzli et al. (2008) used laser-ablation inductively coupled plasma mass spectrometry (LA-ICPMS) on orthogneiss from the Pfaffengrat and identified two magmatic phases of 486 ±27 Ma in cores and 454 ±7 Ma in the rims of zircons. Siegesmund et al. (2021) determined a LA-ICPMS U-Pb zircon age of 479 ±3 Ma, interpreted as a crystallization age, from the amphibole-bearing Engelswand orthogneiss body in the northern Ötztal Nappe. There are still no age data from the Marlengo Slice available.

Schindlmayr (1999) introduced five main groups for the categorization of the granitoids of the Ötztal Complex s. str., while noticing the existence of similar granitoids in the Texel Complex. The groups are from old to young (1) the granitoids of the Central Metabasite Zone, (2) the Winnebach tonalite/granodiorite, (3) the Sulztal granite suite, (4) the granitoids of the Alpeiner type, and (5) the Bassler granite suite. While group 1 to 3 are rare and make up ca. 10 % of the Ötztal granitoids, group 4 and 5 are dominant and make up the rest. The groups are developed by mapped field relationships and show different petrographic and geochemical features. The group 1 granitoids are associated with the older (Cambrian) Central Metabasite Zone. Groups 2–5 are assumed to be of Ordovician to possibly Early-Silurian origin. Group 2 cordierite-tonalites and -granodiorites intruded into the Winnebach metatexite. Group 3 biotite-rich, S-type cordierite-granites are also associated with the Winnebach magmatic complex, but also with the metabasites. Next, group 4 biotite(-hornblende) I-type tonalite, granodiorite to granite intruded in huge volumes into the aforementioned groups. Somewhat later, group 5 S-type granites formed large plutons as the last stage of the Early Paleozoic plutonism in the Ötztal Complex (s. str.). Schindlmayr (1999) differentiated between two variants/subtypes in group 5: two-mica granite gneisses and muscovite (leuco)granite gneisses. After Schindlmayr (1999) the Engelswand orthogneiss body belongs to group 4 and the Pfaffengrat orthogneiss body does not fit well into one of the five groups.

Frisch and Neubauer (1989) defined different Paleozoic terranes in the basement of the Eastern Alps. These terranes were amalgamated in the Variscan orogeny. In the western Austroalpine (west of the Tauern Window), there are parts of the Celtic Terrane, the Speik Terrane and the Noric Composite Terrane. The term Celtic Terrane is used for the basement influenced by an Early Paleozoic magmatic arc. It was welded together from separate terranes by an Early to Middle Ordovician collisional event. The ophiolites of the Speik Terrane have been correlated with the Central Metabasite Zone in the Ötztal Nappe. The Noric Composite Terrane is the Late Ordovician to early Carboniferous passive continental margin consisting of subsiding shelf sequence sediments, Late Ordovician calc-alkaline volcanic rocks, Silurian and Devonian alkaline volcanic rocks, and Carboniferous flysch deposits. After Nievoll et al. (2022), the calc-alkaline porphyroids originated in an extensional domain in the back of the retreating subduction zone and are interlayered with passive margin sediments. In the Ötztal Nappe and surrounding units, most of the basement is assigned to the Celtic terrane. Here, only the Central Metabasite Zone is assigned to the Speik Terrane. The Noric Composite Terrane includes from North to South the Landeck quartz phyllite, the Schneeberg Complex, probably also the Schneeberg Frame Zone and the Laas Series (c.f. Klug and Froitzheim, 2021), an unnamed area of micaschist around Salurn Spitz (Punta Saldura) north of the Matsch Valley (c.f. Hammer, 1926), the Matsch Unit (c.f. Habler et al., 2009), and the quartzphyllite- and marble-bearing parts of the Campo Nappe. Von Raumer et al. (2002) ad-

Unit	Body	Rock Type	Sample	East	North	Analyses
Marlengo Slice	Lower Vernuer	leucocratic orthogneiss	TX12	667458	5177438	RFA
			TX35	667470	5177066	RFA
			TX38	667123	5176591	LA ICPMS, EPMA, RFA
Ötztal Nappe	Sattelspitz	amphibole orthogneiss	TX30	666677	5179050	RFA
			TX44	667242	5178309	LA ICPMS, EPMA, RFA
			TX49	666217	5178079	RFA
	Lodnerhütte	leucocratic orthogneiss	LK17-3	654501	5176244	LA ICPMS, RFA
	Tschigat	orthogneiss	LK17-4	656964	5176324	LA ICPMS, RFA

Table 1: Sample list with coordinates in UTM WGS84 Z:32T.

opted this configuration west of the Tauern Window into an interpretation for the entire Alps. They interpreted the Noric Composite Terrane as continental crust influenced by the opening Paleotethys, the Speik Terrane as remnants of Early Paleozoic oceans, and the Celtic Terrane as part of continental Early Paleozoic metamorphic terranes.

In Ratschbacher and Frisch (1993), the area of micaschists around Praxmar in the northern Ötztal Nappe is part of the Noric Composite Terrane. In the western Ötztal Nappe, the Jaggl Mesozoic together with its basement, the Plawenn Orthogneiss, has been interpreted as a tectonic window (Thöni, 1973; van Gool, 1985; Hammer, 1911) exposing the underlying S-charl Nappe. Froitzheim et al. (1997) described a normal fault at the western boundary of the Jaggl Mesozoic and, therefore, interpreted the Jaggl Mesozoic as a downthrown part of the sedimentary cover of the Ötztal Nappe, and the Plawenn Gneiss as part of the Ötztal basement. The Steinach Nappe is also included in the Noric Composite Terrane (phyllitic and post-Early-Ordovician units) (e.g. von Raumer et al., 2013; Siegesmund et al., 2021). Von Raumer et al. (2013) did not include the Matsch Unit in the phyllitic and post-Early Ordovician units (Noric Composite Terrane), while in Siegesmund et al. (2021), it is part of it. Von Raumer et al. (2013) and Siegesmund et al. (2021) did not consider the Central Ötztal Metabasites as part of the oceanic Speik Terrane but included them in the Celtic Terrane. Post-Ordovician sediments are probably the protoliths of the micashist samples of Siegesmund et al. (2021) from the Schneeberg Complex metasediments (SCHNEE 16-1, PZ 17-05) and from the nearby Ötztal Nappe (PZ 17-03, PZ17-07). Both contain Ordovician magmatic zircon. The authors suggest post-Ordovician deposition only for the Schneeberg Complex.

In summary, the configuration of the Celtic, Speik, and Noric terranes west of the Tauern window and especially in the Ötztal Nappe is only roughly constrained. Based on lithological correlation in our study area, we tentatively assign Schneeberg Complex, Laas Series, Schneeberg Frame Zone and similar micaschists of the Ötztal Nappe (Figs. 1, 2) to the Noric Composite Terrane. The Ordovician orthogneisses and their host rocks represent the Celtic Terrane but are intercalated with the metasediments of the Noric Composite Terrane on the scale of the Ötztal Nappe. The Marlengo Slice has not yet been explicitly assigned to one of these terranes, since detrital zircon data do not yet exist for this unit.

4. Samples

In this study four different orthogneiss bodies from the Texel area were sampled. The samples are listed in Table 1 and the localities are indicated in Figure 2. The samples TX12, TX35, and TX38 are from a leucocratic orthogneiss body from the Marlengo Slice from the lower part of the village Vernuer south of the Saltaus Valley (Lower Vernuer leucocratic orthogneiss). The samples TX 30, TX44, and TX49 are from a folded amphibole-bearing orthogneiss body at the Sattelspitz ridge north of the Saltaus Valley (Sattelspitz amphibole orthogneiss). Sample LK17-3 is from a thin, leucocratic orthogneiss layer close to the Lodnerhütte in the upper Zielbach Valley (Lodnerhütte leucocratic orthogneiss), possibly a dyke connected with the Tschigat orthogneiss. Sample LK17-4 is from the main Tschigat orthogneiss body, also called Partschins orthogneiss (c.f. Bargossi et al., 2010), the largest orthogneiss body of the Texel gruppe. This sample is from Halsljoch, WNW of the Tschigat peak. All samples were taken from bedrock outcrops.

5. Methods

In Table 1 all samples are listed according to the analytical methods performed on them. All analyses were carried out at the Institut für Geowissenschaften of the University of Bonn. Laser ablation inductively coupled plasma mass spectrometry (LA-ICPMS) analyses were carried out on a Resonetics RESOlution M50-E 193nm excimer-laser coupled to a Thermo Scientific ELEMENT XR sector field (SF) ICPMS.

The electron probe micro analyses (EPMA) and cathodoluminescence images of zircons were conducted on a JEOL 8200 Superprobe. The X-ray fluorescence (XRF)

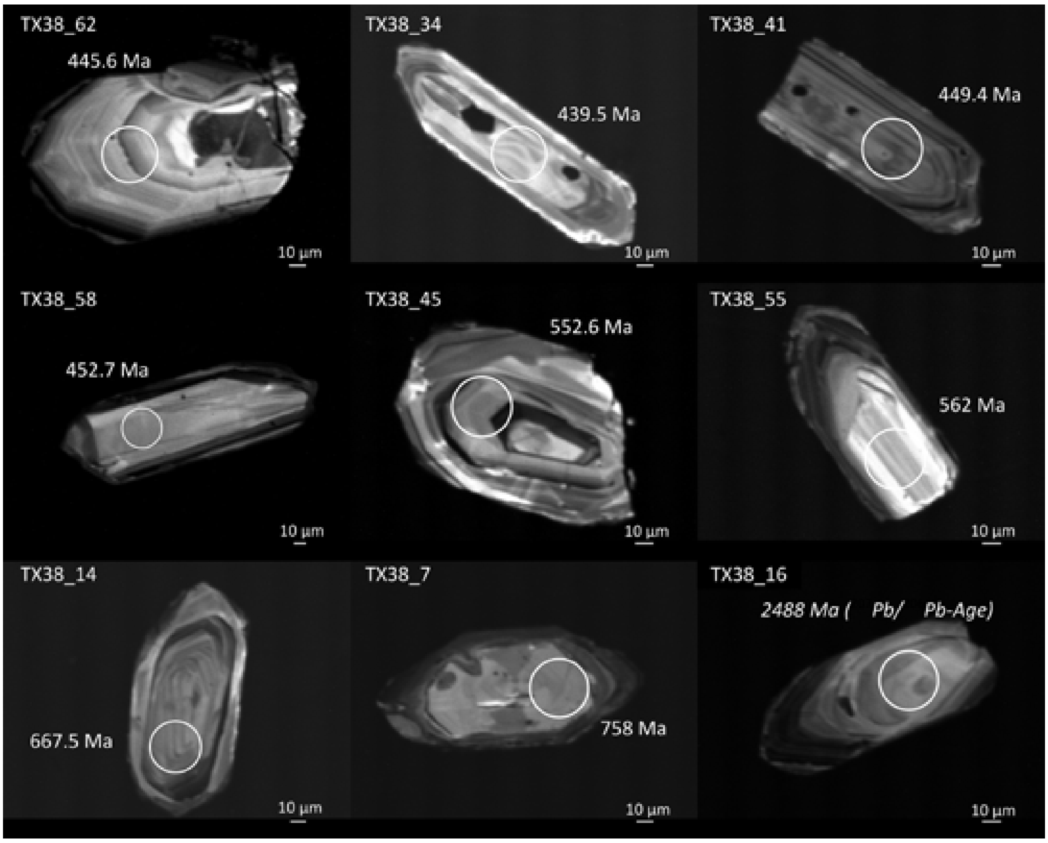

Figure 3: Cathodoluminescence images of exemplatory zircons of TX38. White circles are laser ablation spots marked with measured U^{238}/Pb^{206}-ages unless otherwise marked.

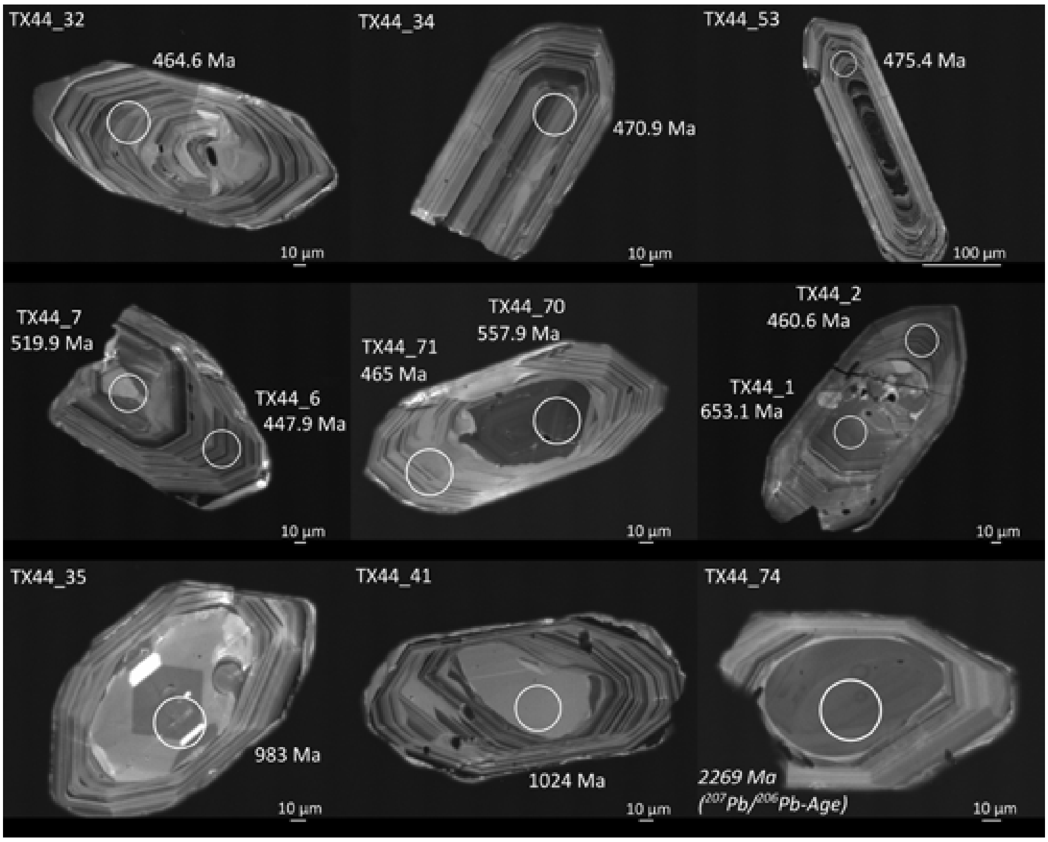

Figure 4: Cathodoluminescence images of exemplatory zircons of TX44. White circles are laser ablation spots marked with measured U^{238}/Pb^{206}-ages unless otherwise marked.

data were measured with a PANalytical-Axios spectrometer, with additional determination of the loss on ignition (LOI). The results of the EPMA and the XRF whole rock geochemistry can be found in the supplementary material (Tables S1, S2 and S3).

U-Pb ages were determined by LA-ICPMS measurements on zircon single grains. After crushing and sieving, mineral separations by magnetic and heavy-liquid techniques were performed. After handpicking of optically clear and inclusion free zircons under the binocular microscope, the grains were mounted in epoxy resin and polished down to half sections. The internal textures were imaged by cathodoluminescence. One hundred to 215 zircons were picked in the 63–125 µm sieve fraction for every sample. The 125–180 µm or 125–250 µm sieve fractions yielded no (TX38) or no more than 30 zircons. In the cathodoluminescence images, zircons with inherited cores were obvious and frequent in all samples. The presence and size of internal domains influenced the selection of ablation spot sites, and the grain size that for single-domain zircons. Although the spot sites were concentrated on the domains of latest magmatic growth, core domains were also selected.

U-Pb data for zircon was collected following an adaption of methods previously used in this lab (Nilius et al., 2016; Pohl et al., 2018). The instrumental and analytical details for the different samples are provided in the online supplement (Tables S4, S5 and S6).

For Laser-induced downhole fractionation, mass bias and instrument drift were corrected by normalizing to the Plešovice zircon reference material (Sláma et al., 2008). The reduction scheme VizualAge 2015.06 in Iolite 2.5 was used for raw-data processing (Paton et al., 2011; Petrus and Kamber, 2012; Chew et al., 2014). Age plotting and calculation were carried out on the Isoplot plugin for Excel (Ludwig, 2012) and the substitute program IsoplotR (Vermeesh, 2018). No common-Pb correction was performed, due to low ^{204}Pb count rates indicating an insignificant common-Pb influence. The extraction of two dates from single spot analyses was occasionally possible, due to ablation of multiple discrete growth domains in zircons. Analyses were selected for U-Pb age calculation after excluding measurements of inherited cores and mixed ages due to partly ablated older inherited cores or younger metamorphic rims. Additional criteria for excluding measurements were discordance (ca. ±10 %) and Th/U ratios (<<0.1) in combination with apparent mixed ages based on zircon texture in cadoluminescence images, isotope ratio shift during ablation (no plateau) and the post-sequence observed laser ablation pit position. A systematic uncertainty of 1.5 % was propagated by quadratic addition into the final ages of the unknown populations.

6. Petrography and mineral chemistry

6.1. Lower Vernuer leucocratic orthogneiss

This leucocratic orthogneiss of the Marlengo Slice (c.f. Bargossi et al., 2010; Klug, 2016) is white to light green, has a medium grainsize and an almost granite-like appearance. The deformation of these rocks varies in the Saltaus Valley from dominantly brittle, close to the Forst Fault cataclastic, to subordinately ductile with weak to moderate foliation. The Lower Vernuer leucocratic orthogneiss contains feldspar, quartz and white mica with minor chlorite and calcite. Accessories are apatite and zircon. Feldspars are microcline (ab_{0-3}) with typical twinning as large porphyroclasts and fine-grained albite (an_{0-4}). White mica is muscovite with layers of chlorite. Calcite is found in veins.

6.2. Sattelspitz amphibole orthogneiss

The amphibole orthogneiss from the Saltaus Valley in the Texel Complex is light grey, has a fine to medium grainsize and shows moderate ductile deformation with foliation and flaser structure (c.f. Bargossi et al., 2010; Klug, 2016). It contains amphibole, plagioclase, K-feldspar, biotite, quartz, titanite, clinozoisite, epidote, chlorite, white mica, calcite, garnet, allanite and zircon. The amphiboles are magnesio-hornblende with rims of pargasitic and actinolitic composition. Iron is 90–100 % Fe^{2+} and Mg# is 0.50-0.59 in the magnesio-hornblende. Plagioclase is andesine (an_{32-38}) and abundant K-Feldspar (ab_{0-5}) gives evidence for a granodioritic protolith composition. The phases of the epidote-clinozoisite-series have varying Fe-contents of 1.9–5.8 %. Biotite (phl_{46-50}) is partly replaced by chlorite (diabantite according to K content). Otherwise, chlorite is mainly pychnochlorite or ripidolite. Sericitic white micas have compositions of phengitic muscovite. The amphibolite-facies paragenesis of amp, bt, ti, clz and ep forms the main foliation which is overgrown by greenschist-facies chlorite and sericite.

6.3. Lodnerhütte leucocratic orthogneiss

The Lodnerhütte leucocratic orthogneiss is a few tens of meters thick layer of light coloured orthogneiss with augen structure (c.f. Bargossi et al., 2010). It is imbedded in paragneisses. Except for the augen, the orthogneiss shows a small to medium grain size and a strong foliation. The sample LK17-3 comprises K-feldspar (microcline), plagioclase, quartz, white mica, biotite, chlorite, apatite, and zircon in thin section. Mineral compositions have not been measured.

6.4. Tschigat orthogneiss

The Tschigat orthogneiss body consists of coarse grained, biotite-rich granite gneiss with K-feldspar augen structure (c.f. Schindlmayr, 1999; Bargossi et al., 2010). It shows moderate ductile deformation with wavy foliation around the abundant augen. In thin section the sample LK17-4 exhibits K-feldspar (microcline) and plagioclase, sericitic alteration, quartz and chloritized biotite. Mineral chemistry has not been measured.

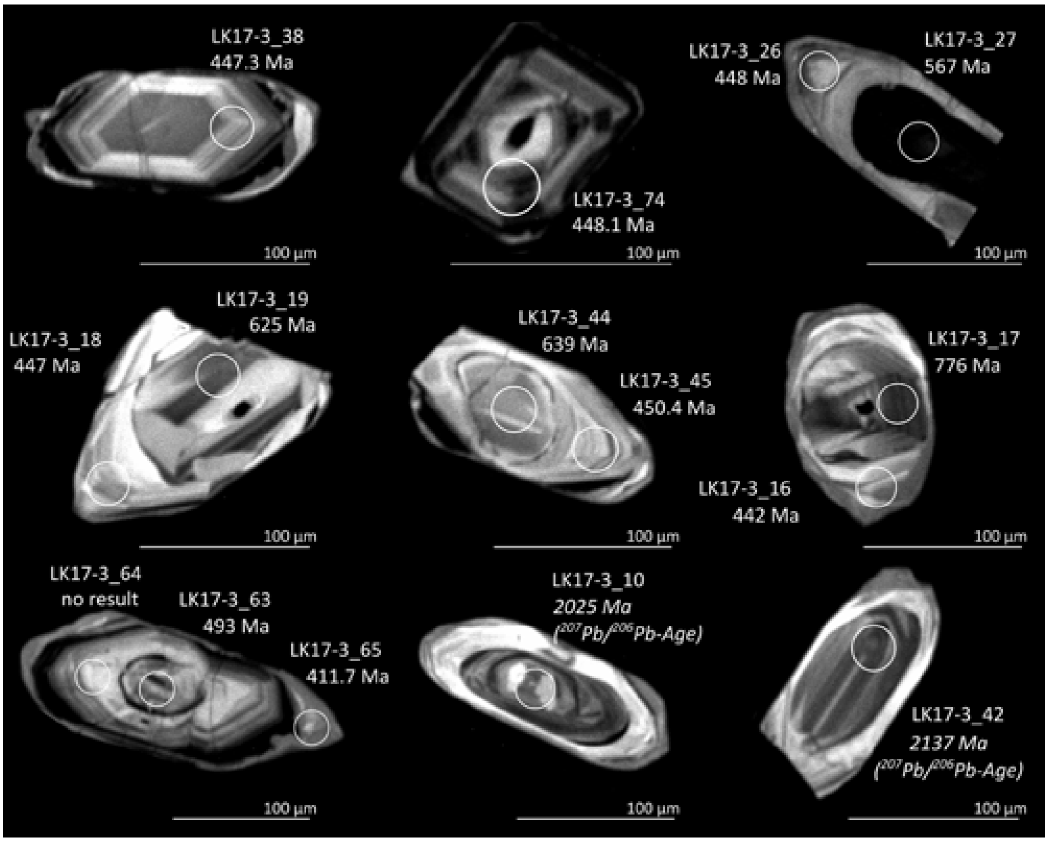

Figure 5: Cathodoluminescence images of exemplatory zircons of LK17-3. White circles are laser ablation spots marked with measured U^{238}/Pb^{206}-ages unless otherwise marked.

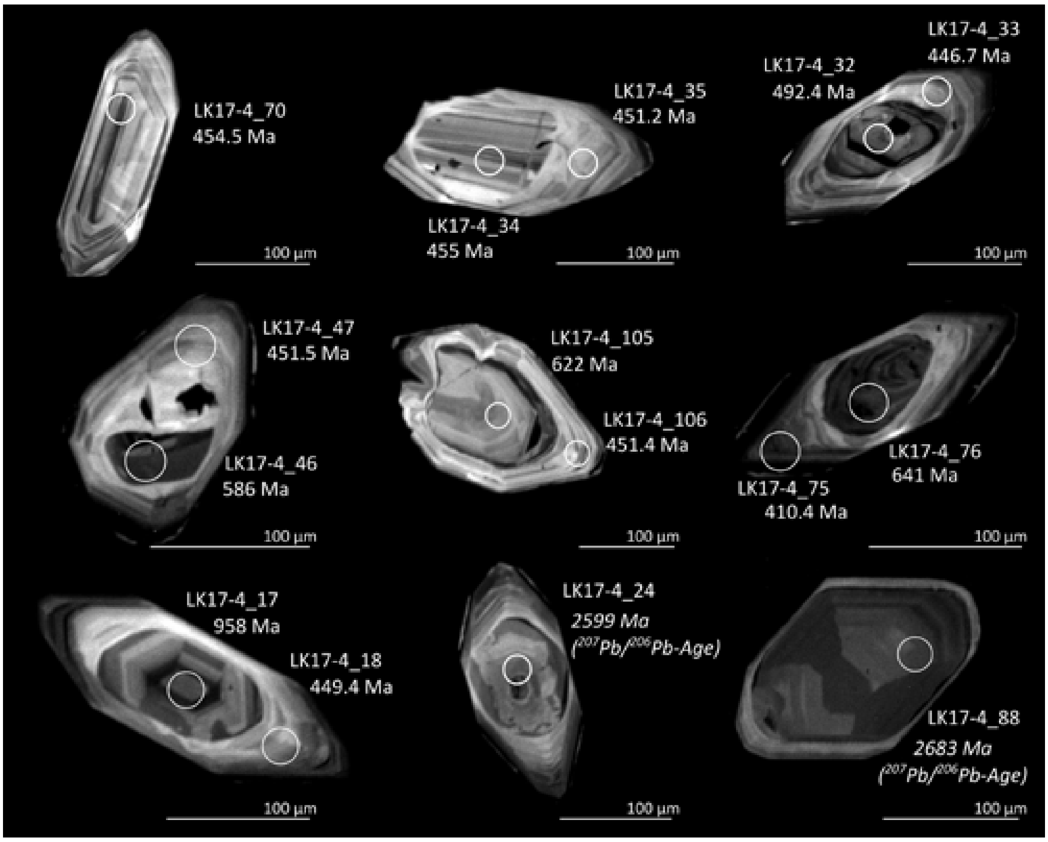

Figure 6: Cathodoluminescence images of exemplatory zircons of LK17-4. White circles are laser ablation spots marked with measured U^{238}/Pb^{206}-ages unless otherwise marked.

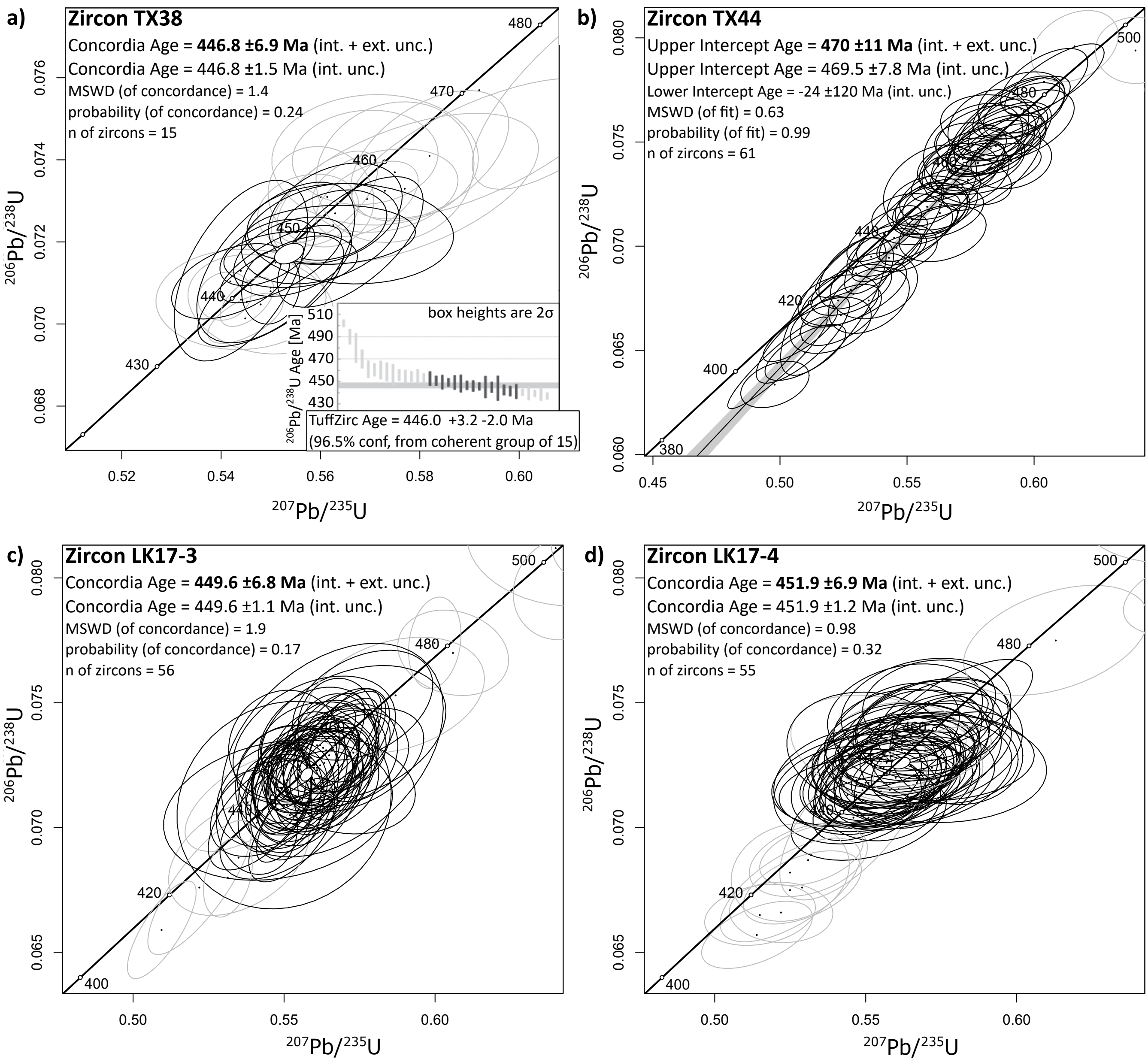

Figure 7: Concordia ages for last magmatic growth in samples **(a)** TX38, **(b)** TX44, **(c)** LK17-3, **(d)** LK17-4.

7. Zircon U-Pb geochronology

7.1. Magmatic protolith ages

7.1.1. TX38 (Lower Vernuer leucocratic orthogneiss)

Zircons in TX38 are 63 to 125 µm in size and have roundish to prismatic forms with proportions of 1:1 to 1:4. The zircons show cracks and some, especially prismatic grains, are just fragments. CL images are dark and low in contrast but internal textures are recognizable (Fig. 3). Core domains as well as the domain of last magmatic growth show oscillatory zoning patterns (Corfu et al., 2003). Cores are recognizable in about 55 % of the polished zircons. The zircons are rimmed by a light zone without any texture. These probably metamorphic rims are up to ca. 10 µm thick. The selection of concordant data points without identifiable influences by core or rim domains shows a too broad scatter for a protolith intrusion age calculation. A statistically robust selection was obtained with the TuffZirc algorithm of Ludwig and Mundil (2002). After exclusion of analyses with anomalously high uncertainties it seeks a population of ranked $^{206}Pb/^{238}U$ dates with a probability of fit >0.05. The resulting population of 15 analyses gives a median $^{206}Pb/^{238}U$ age of 446.0 +3.2/-2.0 Ma with an asymmetric 96.5 % confidence level. This population yields a concordia age of 446.8 ± 6.9 Ma (int. + ext. uncertainty) (Fig. 7a).

7.1.2. TX44 (Sattelspitz amphibole orthogneiss)

The analysed zircons in TX44 are 63 to 250 µm in size and grains are mainly prismatic with length ratios up to

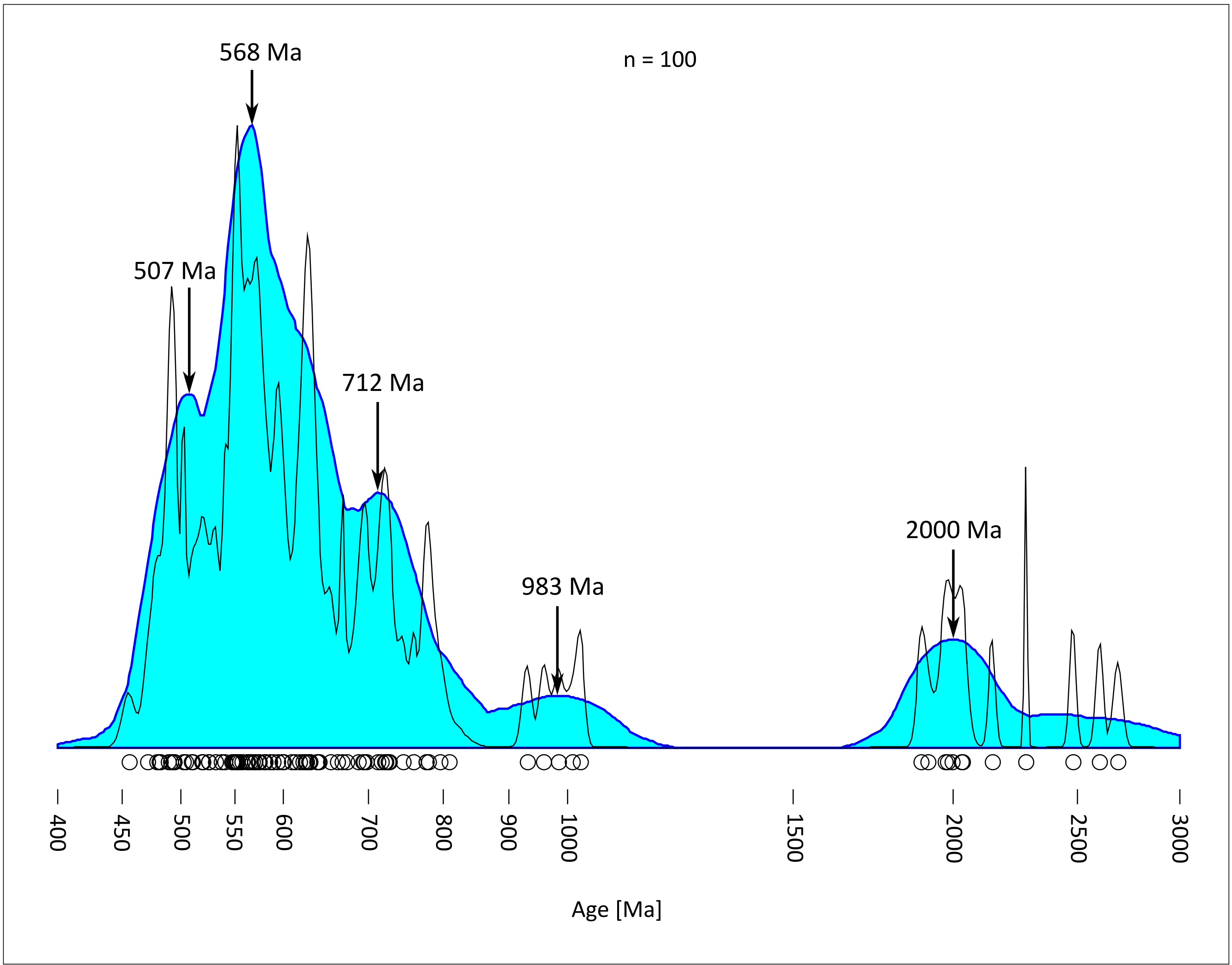

Figure 8: Inherited zircon cores combined from samples TX38, TX44, LK17-3 and LK17-4 in a Kernel Density Estimation (blue) and a probability density plot (black). Cores younger than 1500 Ma are plotted with U^{238}/Pb^{206}-ages, cores older than 1500 Ma with Pb^{207}/Pb^{206}-ages.

1:4. The zircons are often cracked and partly fragmented. In CL images rare metamict zones in grain centres are visible (Fig. 4). Internal structures show often complex core domains surrounded by oscillatory patterns. Major cores have internal structures varying from clear oscillatory zoning to weak or texture-free patterns. In about 70 % of the zircons, cores are visible. The grains exhibit a fine metamorphic rim.

Analyses representative of the last magmatic growth are aligned on a regression line indicating recent Pb-loss. The upper intercept at 470 ±11 Ma (int. + ext. uncertainty) reports the age of the last magmatic growth stage (Fig. 7b). Analyses with values offset from this regression line were excluded from the calculation.

7.1.3. LK17-3 (Lodnerhütte leucocratic orthogneiss)

The zircons from sample LK17-3 are from the 63 to 180 µm sieve fraction. They are short to moderately prismatic from 1:1.5 to 1:4. The zircons are partly fragmented or have irregular forms. Complex core domains, resorption, overgrowth, and rim structures are visible in CL images (Fig. 5). In about 60 % of zircons, cores are visible. A few µm wide, light-colored rims surround the outermost oscillatory patterned zones. The measurements representing the last magmatic zircon growth yield a concordia age of 449.6 ± 6.8 Ma (int. + ext. uncertainty) (Fig. 7c).

7.1.4. LK17-4 (Tschigat orthogneiss)

Zircons from 63 to 180 µm were extracted from sample LK17-4. The zircons are mostly moderately prismatic with aspect ratios of 1:2 to 1:4. Needle-like zircons with ratios up to 1:8 and needle or prism fragments are frequent. CL images are similar to those of LK17-3 and show complex core, resorption, overgrowth, oscillatory zoning, and fine rim structures (Fig. 6). Cores occur in up to 85 % of the zircons. The concordia age of last magmatic growth is 451.9 ± 6.9 Ma (int. + ext. uncertainty) (Fig. 7d).

7.2. Metamorphic ages

In TX38, young ages are interpreted as influenced by the partial ablation of rims. These ages are excluded by the TuffZirc algorithm. The rims are too thin to determine an age. In TX44, young ages influenced by partial ablation of rims and offset from the recent Pb-loss regression line were excluded from the calculations. In LK17-3, measurements on metamorphic rims resulted in younger mixed ages down to about 410 Ma, but an age of the metamorphic growth could not be extracted. In LK17-4, the influence of metamorphic rims results in younger (mixed?) ages down to 366 Ma. Again, no metamorphic age could be extracted.

7.3. Inherited zircon ages

All samples exhibit older zircon cores identifiable by textures in CL images. Figures 3–6 show representative zircons with cores and ages of the laser ablation spots for the four samples. Zircon cores were dated when they were large enough for the spot size used (33 µm or 26 µm). A range of ages could be determined in zircon cores which are slightly to significantly older than the age of last magmatic growth. The youngest cores are within uncertainty identical to the age of the last magmatic growth. For example, the sample spots LK17-3_34 (the youngest dated core) and LK17-3_35 (last magmatic growth) have $^{206}Pb/^{238}U$ dates of 455 Ma and 452 Ma, respectively. The oldest zircon core was found in sample LK17-4 with a $^{207}Pb/^{206}Pb$ date of 2683 ±42 Ma. The identified, dated, and concordant cores of all four samples have been plotted together, similar to detrital zircons in a Kernel Density Estimation (KDE) plot in combination with a probability density plot (PDP) with the program DensityPlotter (Vermeesh, 2012) (Fig. 8). Here, the $^{206}Pb/^{238}U$-ages are plotted for the ages below 1500 Ma. Above 1500 Ma, the $^{207}Pb/^{206}Pb$-ages are plotted because they are more robust in that age range. Since only concordant ages are used, mixed ages and ages with Pb-loss (in sample TX44) are left out. In this way 100 zircon core ages are plotted. The ages are not plotted separately for each sample because on one hand, the low number of zircon cores would lead to weak statistics. On the other hand, there are no significant differences between the samples with respect to zircon core ages.

The zircon cores show a continuous age distribution between ca. 450 Ma and ca. 800 Ma, with the youngest peak at ca. 490 Ma, a minimum at ca. 510–540 Ma, the overall highest abundance between ca. 540–580 Ma, and further peaks at ca. 610 Ma and 800 Ma. A small cluster of ages occurs at ca. 1000 Ma. The oldest zircon cores are between ca. 1800 Ma and ca. 2700 Ma, with a peak at ca. 2000 Ma.

8. Whole rock geochemistry and tectonic environment

Assuming isochemical metamorphism, the geochemistry of the orthogneisses can be used to characterize their magmatic protoliths. All samples show typical granitoid composition. We use discrimination schemes for major elements and combine our data with the data from the Texel area of Bargossi et al. 2010 (and references therein) and from the Ötztal Complex s. str. of Schindlmayr (1999) for comparison. We present these in the discrimination

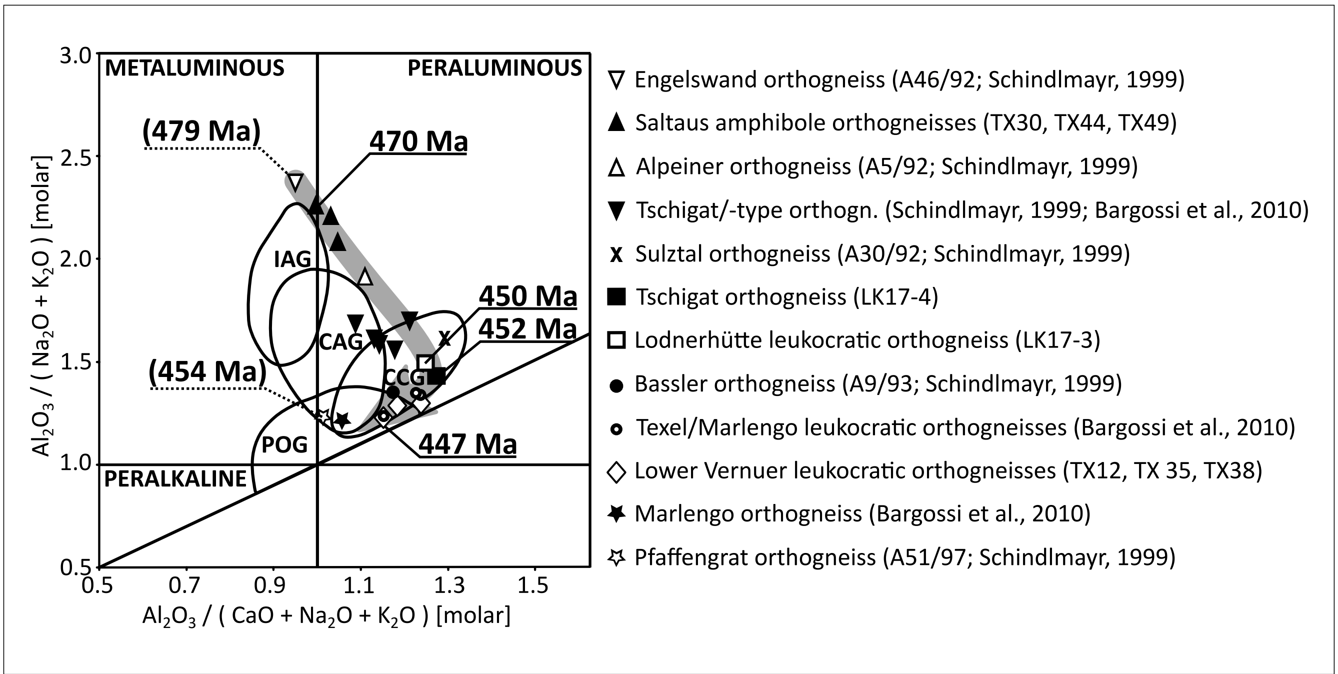

Figure 9: Discrimination diagram of granitoids after Maniar and Piccoli (1989) with geochemical data from orthogneisses of this study, Bargossi et al. (2010) and Schindlmayr (1999). Ages for the samples TX38, TX44, LK17-3 and LK17-4 are from this study. Ages in brackets are from Klötzli et al. (2008) (454 Ma) and Siegesmund et al. (2021) (479 Ma). The arrow marks the temporal differentiation trend.

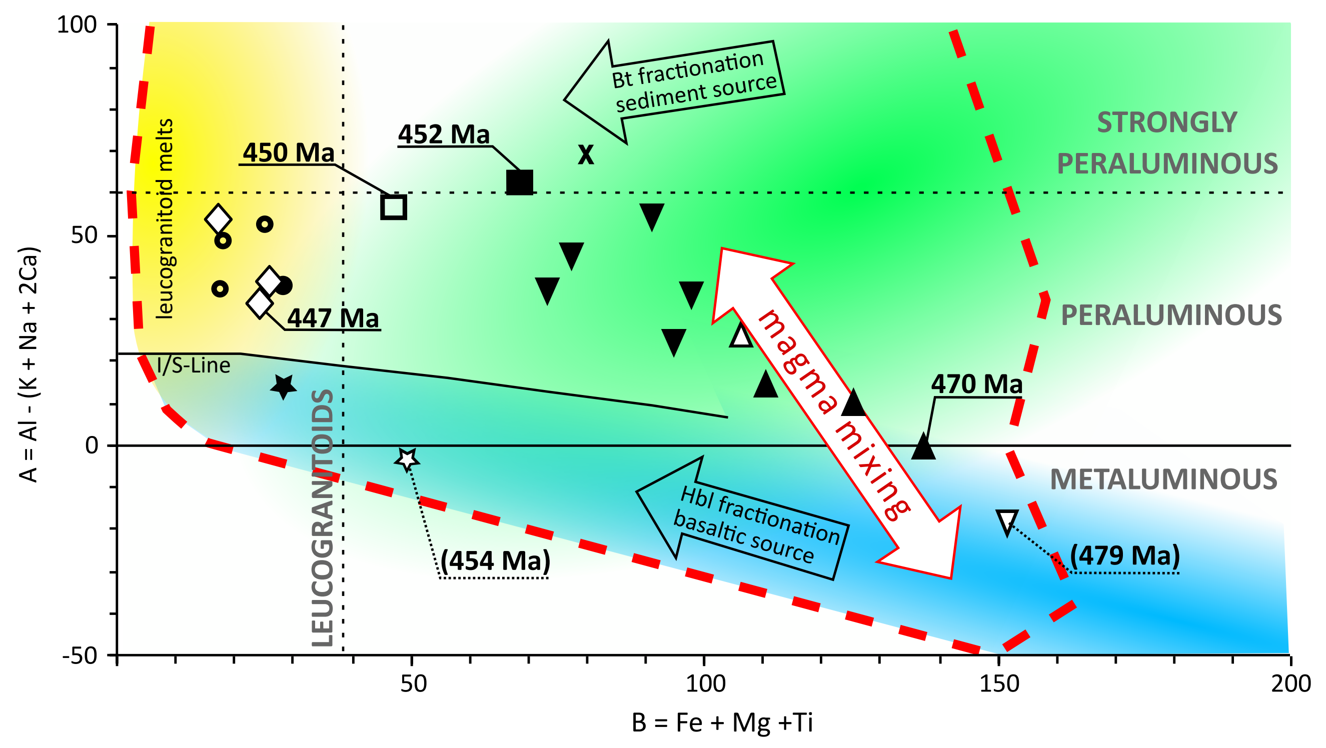

Figure 10: Discrimination diagram after Debon and Le Fort (1988) and Zurbriggen (2015, 2020) with data from orthogneisses of this study, Bargossi et al. (2010) and Schindlmayr (1999). Ages for the samples TX38, TX44, LK17-3 and LK17-4 are from this study. Ages in brackets are from Klötzli et al. (2008) (454 Ma) and Siegesmund et al. (2021) (479 Ma). Colored fields are leucogranitoid melts (yellow), sediments (green), high-temperature I-type granitoids (blue) and low-temperature I- and S-types (red line). The I/S-line is used after Villaseca et al. (1998). Symbols as in Figure 9.

schemes of Maniar and Piccoli (1989; see also Schulz et al., 2008), and of Debon and Le Fort (1988) and Villaseca et al. (1998; see also Zurbriggen, 2020). In the diagrams (Figs. 9 and 10), the samples are grouped by orthogneiss type and location. The above-described LA-ICPMS zircon U-Pb ages are also plotted. Ages for the samples TX38, TX44, LK17-3 and LK17-4 are from this study. Note that the ages in brackets from Klötzli et al. (2008) and Siegesmund et al. (2021) are not from the same samples as the geochemical data of Schindlmayr (1999), but from the same orthogneiss body.

For the discrimination diagram after Maniar and Piccoli (1989), the molar weight ratios of $Al_2O_3/(Na_2O + K_2O)$ and $Al_2O_3/(CaO + Na_2O + K_2O)$ were calculated from the XRF wt-% data (Fig. 9). Maniar and Piccoli (1989) assign compositional fields to tectonic environments. These are island arc granitoids (IAG), continental arc granitoids (CAG), continental collision granitoids (CCG) and post-orogenic granitoids (POG).

The Sattelspitz amphibole orthogneiss and the Engelswand orthogneiss samples plot closest to the IAG composition field. The Alpeiner orthogneiss plots close to the CAG composition field. The samples from the Tschigat and Tschigat-type orthogneisses including LK17-4 plot in an area overlapping the CAG and CCG fields. The leucocratic orthogneisses from the Ötztal, Texel and Marlengo units plot in the CCG and partly in the POG field. The sample LK17-3 (Lodnerhütte leucocratic orthogneiss) and the Sulztal orthogneiss plot in the CCG field. The Marlengo orthogneisses, the Bassler orthogneiss, and the Pfaffengrat orthogneiss plot in the area where CAG, CCG, and POG overlap.

Following Zurbriggen (2015, 2020), we used the discrimination scheme of Debon and Le Fort (1988) with additions from Villaseca et al. (1998). The rocks are discriminated by their metaluminosity and peraluminosity (A-value: Al – (K + Na +2Ca)) versus their felsicity and maficity (B-value: Fe + Mg + Ti) (Fig. 10). For the calculation using wt-% of oxides, molecular weight, and millicationic values, see Debon and Le Fort (1988). The scheme is primarily descriptive without standard tectonic interpretations, but can identify trends of magmatic processes (Zurbriggen, 2020). In the diagram (Fig. 10) areas of the typical range of compositions for different rock types are depicted after Zurbriggen (2020). Outlined in red are low-temperature I- and S-type granitoids. The green field represents the melting sediments (pelites, greywackes). Highly fractionated melts solidify as leucogranitoids (yellow). The blue field represents the CAFEM-field, a type of magmatic association composed of metaluminous rocks (Debon and Le Fort, 1988) which have a basaltic melt source and are high temperature I-type granitoids. Additionally, the I/S-line (Villaseca et al., 1998) divides typical I- and S-type granitoid compositions.

The Sattelspitz amphibole orthogneiss, the Engelswand orthogneiss, and the Alpeiner orthogneiss samples have the highest B-values (ca. 105–150) and plot in the moderately peraluminous field close to the low peraluminous granitoid field and to the metaluminous field. The Tschigat and Tschigat-type orthogneisses and the Sulztal orthogneiss plot in a more felsic area (B-value: ca. 65–95) and are higher in peraluminosity. They reach from the moderately peraluminous to the highly peraluminous field. The Lodnerhütte leucocratic orthogneiss plots not in but close to the leucogranitoid field (B-value: ca. 50) and in the highly peraluminous field. The other leucocratic orthogneisses (Texel/Marlengo) plot in the leucogranitoid field (B-value: ca. 15–30) and in the highly felsic granitoid field. The Marlengo orthogneiss of Bargossi et al. (2010) and the Pfaffengrat orthogneiss plot under the I/S-Line in the I-type field, while all other orthogneisses except for the Engelswand orthogneiss plot more or less above in the S-type field.

9. Discussion

9.1. Compositional and temporal evolution of magmatism

The zircon ages of the last magmatic growth zones in the orthogneisses are interpreted as the emplacement ages of the granitoid protoliths. In Figure 11, the zircon ages are plotted on a time axis with their uncertainty bars (int. + ext. uncertainty). Although sample TX44 has a higher age uncertainty, it is clearly older than the other samples, as the uncertainties do not overlap. The samples LK17-4, LK17-3 and TX38 have a smaller age uncertainty but lie closer together in time, which results in significant overlap within uncertainty. In the following, we discuss the correlation of the temporal evolution with the geochemical variations.

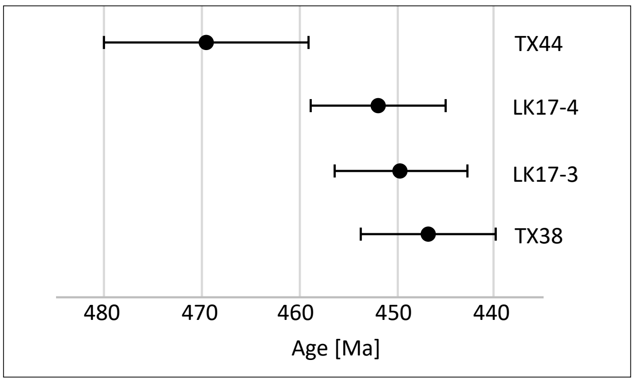

Figure 11: Time scale of magmatic growth concordia ages of samples TX38, TX44, LK17-3 and LK17-4 with 2σ uncertainty-bars.

Based on rock descriptions and compositional characteristics, we correlate the Sattelspitz amphibole orthogneiss (470 Ma) with group 4 after Schindlmayr (1999). The Lodnerhütte leucocratic orthogneiss (450 Ma) and the Lower Vernuer leucocratic orthogneiss (447 Ma) fit the characteristics of the youngest group 5. Schindlmayr (1999) was undecided if the briefly described Tschigat orthogneiss belongs to the older group 3 (based on zircon typology) or the younger group 5 (based on appearance similar to the Silzer granite gneiss in the northern Ötztal Complex). Our geochemical data is also unconclusive. The younger magmatic protolith age of the Tschigat orthogneiss (452 Ma) relative to the Sattelspitz amphibole orthogneiss (group 4) shows that the Tschigat orthogneiss belongs to group 5. This means that our age data are in harmony with the observations of Schindlmayr (1999).

In the diagram after Maniar and Piccoli (1989) (Fig. 9), an arrow shows the observed chemical and chronological evolution trend of the orthogneisses in the Ötztal, Texel, Tschigat, and Marlengo area. Our above-described ages from the LA-ICPMS U-Pb zircon dating of the samples TX44 (470 Ma), LK17-4 (452 Ma), LK17-3 (450 Ma), and TX38 (447 Ma) are indicated in the diagram. These ages outline a trend from the older Sattelspitz amphibole orthogneiss over the Tschigat(-type) orthogneisses to the younger leucocratic orthogneisses of the Ötztal unit and the youngest of the Marlengo unit. From the Tschigat(-type) to the Marlengo orthogneisses, the evolution turns in the direction of the POG field. Combined with the groups and geochemistry of Schindlmayr (1999), the LA-ICPMS ages of 479 Ma from the Engelswand (Siegesmund et al., 2021) and of 454 Ma from the Pfaffengrat (Klötzli et al., 2008) orthogneiss bodies both support our observed Ordovician differentiation trend (Figs. 9 and 10). Unlike the LA-ICPMS age data, other age data do not resolve the complex internal zircon textures sufficiently.

Schulz et al. (2008), in an equivalent diagram after Maniar and Piccoli (1989) for the Austroalpine basement south of the Tauern Window, drew the early part of their chemical and chronological evolution trend similarly to our trend, but it ends with a turn in the opposite direction, away from the POG field in the direction of meta-porphyroids with higher Al to Ca + Na + K ratios. This seems inconsistent, as the meta-porphyroids of Schulz et al. (2008) are older (ca. 479-473 Ma) than the youngest (ca. 448 Ma) orthogneisses with a less aluminous chemistry. Generally, our data confirms the geochemical temporal evolution in the Ordovician magmatites south of the Tauern window (Schulz et al., 2008) and in the larger area (e.g., von Raumer et al., 2002; Spiess et al., 2010). This supports the existence of a general geochemical trend in the Ordovician magmatites west of the Tauern window (Ötztal Nappe, Texel area). Von Raumer et al. (2002) and Spiess et al. (2010) also use the discrimination after Maniar and Piccoli (1989) and similarly suggest a trend from an active margin to a collisional setting for Ordovician magmatites on the northern Gondwana margin. They did not consider an Alaskan-type accretionary orogen.

Zurbriggen (2015, 2020) used the diagram of Debon and Le Fort (1988) to support the idea of an Alaskan-type accretionary orogen. One main character of Alaskan-type accretionary orogens is the high sediment input into the subduction zone (e.g., Zurbriggen, 2017). This sediment is seen as the main melt source for the granitoids. Similar to the samples of Zurbriggen (2015, 2020), most of our samples show a sediment melt origin by plotting in the sediment field (green) or represent more fractionated leucocratic products of melted sediments. The Sattelspitz amphibole orthogneiss samples plot in an area between the sediments (green) and the CAFEM field (blue) in the prolongation of the I/S-line. The per- to metaluminous character shows the influence of a basaltic melt source. On the other hand, the abundance of inherited zircon cores in the zircons of the Sattelspitz amphibole orthogneiss (TX44) suggests sediments as melt source. Magma mixing is a possible explanation for the formation of metaluminous granitoids with inherited detrital zircons. Basaltic melts and anatectic felsic melts commonly do not mix due to different temperatures and the resulting viscosity contrast (Barker et al., 1992). After Zurbriggen (2020), the more fractionated CAFEM-series of basaltic origin can mix with the sediment-derived melts, which occurs at temperatures of ca. 850 °C (Zurbriggen, 2015; see also Vielzeuf and Holloway, 1988). The main fractionation process in the CAFEM-series is hornblende fractionation (Debon and Le Fort, 1988).

While Zurbriggen (2020) describes the development of the per- and metaluminous granitoids as contemporaneous, our data show a temporal evolution from metaluminous to peraluminous granitoids and an increasing felsicity over time. This differentiation trend is here observed exclusively in the Ordovician magmatic cycle, while Zurbriggen (2020) describes an evolution from an I-type-dominated Cadomian orogeny (Andean-type continental arc) to an S-type dominance during the Cenerian orogeny (Alaskan-type subduction-accretion complexes). The late Precambrian to Cambrian Cadomian orogeny precedes the Ordovician Cenerian orogeny (Schulz et al., 2008; Zurbriggen, 2020). Here, we identified a more short-lived differentiation trend restricted to the Ordovician magmatic cycle.

9.2. Inherited ages

The age distribution of zircon cores leads to the following considerations. The melt source of the sampled orthogneisses shows an affinity to the Northeast Africa-Arabia Zircon Province (Stephan et al., 2018), as far as the older part (>700 Ma) of the age distribution is concerned. The younger part of the age distribution (<700 Ma) remains to be interpreted. The chemistry of the orthogneisses implies a sedimentary melt source or a melt source in S-type granitoids or a combination. The older Sattelspitz amphibole orthogneiss has a minor basaltic/basic melt source component that does not seem to change the zircon distribution and abundance much. One explanation for the young inherited zircons (ca. 455–500 Ma) in the slightly younger orthogneisses could be that they stem from melted sediments where the youngest zircons are detrital and define the maximum deposition age. These sediments would have been deposited shortly before melting, i.e. contemporaneously with the Ordovician magmatic phase. This is conceptualized for the Northern Gondwana margin by the Cenerian Alaskan-type subduction-accretion orogeny after Zurbriggen (2017). Alternatively, multi-phase melting and zircon growth in a single melt body as well as assimilation of older zircons from neighboring Early Ordovician granitoids could explain the inherited Ordovician zircon cores. This can also be assumed for the I-type Pfaffengrat orthogneiss body with a zircon core age of 486 Ma and a magmatic rim age of 454 Ma (Klötzli et al., 2008). The highest peak of inherited zircons of 540–580 Ma is attributed to the Cadomian arc magmatism. Arc related and (calc-)alkaline magmatites are abundant in the Austroalpine basement south of the Tauern Window and in the Silvretta basement and have Ediacaran to Cambrian ages (ca. 520–590 Ma) (Siegesmund et al., 2021; and references therein).

Apart from the possibly assimilated Ordovician magmatites, it can be assumed that the melt source was mainly composed of sediments with the observed zircon provenance pattern including the highest peak of ca. 540–580 Ma old zircons. Detrital zircon data from the Ötztal basement metasediments indicate Cambrian maximum deposition ages (Siegesmund et al., 2021). The magmatic hiatus from ca. 500 to 520 Ma (Siegesmund et al., 2021; Stephan et al., 2019) is visible as a decrease in the zircon age distribution (Fig. 8).

In an active margin setting sediments incorporate young magmatic zircons of the active margin in a high proportion (Cawood et al., 2012). The Ötztal basement metasediments do not show Ordovician zircons and only very few Cambrian/post-Cadomian zircons (Siegesmund et al., 2021; and own unpublished data). The Ötztal basement metasediments are therefore, assuming an active margin, older than Ordovician magmatism. There seems to be a significant age gap between the deposition of the Cambrian sediments and their being intruded by Ordovician magmatism.

9.3. Tectonic framework of Ordovician magmatism

The Ordovician and pre-Ordovician basement of the Ötztal Nappe is dominated by metasedimentary rocks. The Ordovician orthogneisses also show a major sedimentary influence. These sediments are seen as part of the super-large early Paleozoic peri-Gondwanan greywacke-pelite series stemming from the Gondwana mainland (Zurbriggen, 2017) and being deposited after the Cadomian magmatic phase. The nature of the Cambrian post-Cadomian Gondwana margin is unresolved. Stephan et al. (2019) assume a passive margin, also during the Ordovician. A majority of authors is in favor of an active margin, but subduction characteristics are not conclusive. In general, a continuation from Cadomian to Ordovician subduction is assumed (e.g. Zurbriggen, 2017; Siegesmund et al., 2021; Neubauer et al., 2022; Finger and Riegler, 2023).

The coexistence of Cadomian (Late Ediacaran - Early

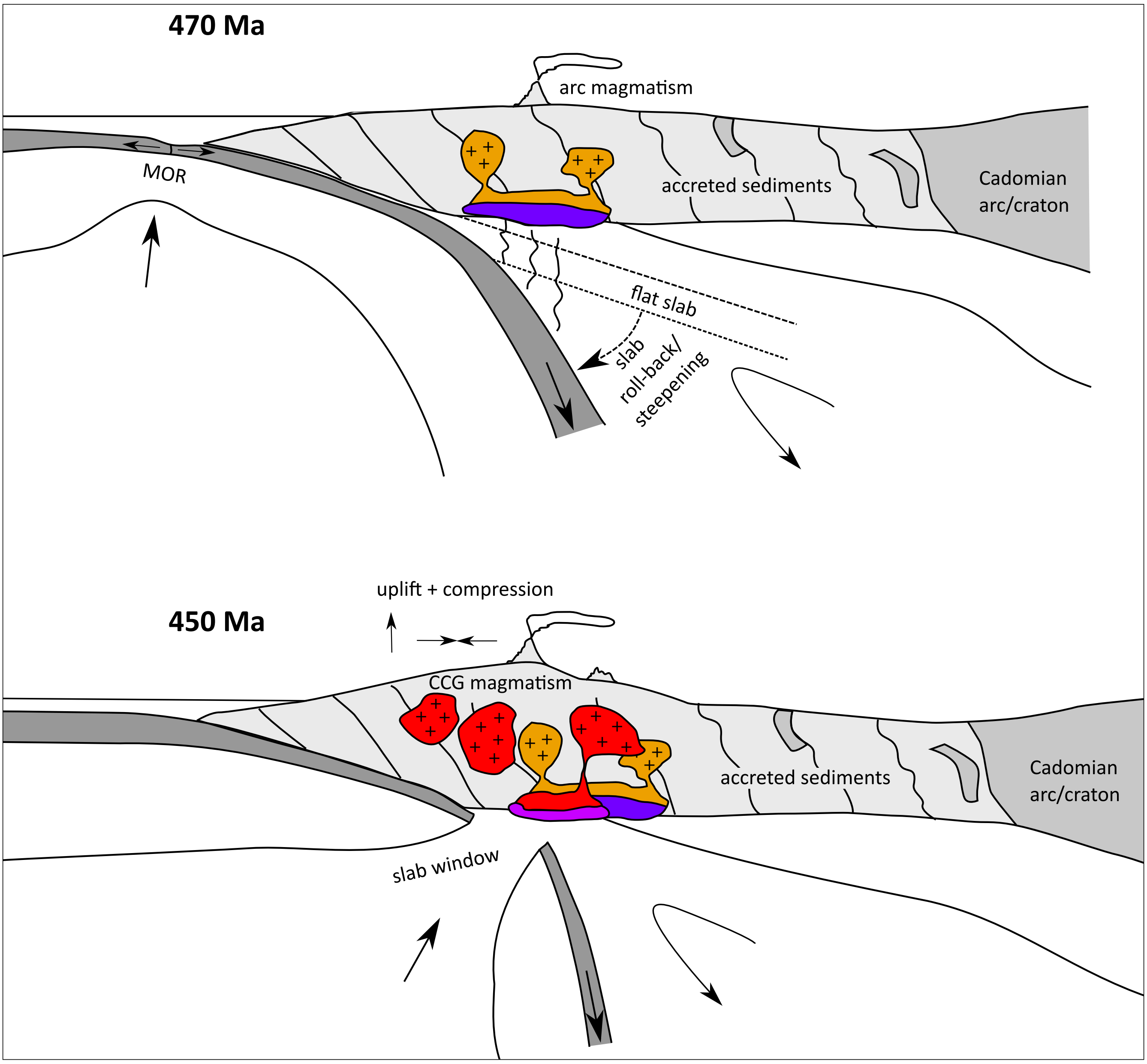

Figure 12: Tectonic model of the Ordovician magmatism in the Texel complex for the time steps 470 Ma and 450 Ma, with underplating basaltic melts (purple and pink) and emplaced granitoids (orange and red), respectively. The observed differentiation trend is linked to slab steepening/roll-back and mid ocean ridge subduction. See text for details.

Cambrian) magmatites and younger Late Cambrian to Ordovician granitoids in the Silvretta Complex, the Schladming Complex, and the Northern Defereggen Complex (Neubauer et al., 2022) contradicts the model of Zurbriggen (2017), where the trench and the magmatic arc are moving away from older arc magmatites, older accreted sediments and the cratonic mainland by the oceanward advance of the continental margin. Similarly, in the Ötztal Complex the Early Cambrian Central Metabasite Zone coexists with the Late Cambrian to Ordovician granitoids. However, the metabasites might alternatively be interpreted as a later obducted ophiolite (Neubauer et al., 2022).

The host rock for the Ordovician magmatism of the Ötztal Nappe was a continental crust consisting primarily of Cambrian clastic sediments at the northern margin of Gondwana near Northeast Africa and Arabia, as indicated by zircon provenance. The increase of magmatic activity, which led to the Ordovician magmatic peak, started with partial melting of these sediments and the formation of migmatites at ca. 490 Ma (Klötzli-Chowanetz et al., 1997). Ordovician mid-ocean ridge (MOR) subduction starting at c. 470–480 Ma may explain the increased magmatic activity by additional heat input (e.g., Stampfli, 2000; von Raumer et al., 2002; Schulz et al., 2008; Zurbriggen, 2015). An approaching MOR causes the steepening of the subducting slab and/or slab rollback (e.g., Salze et al., 2018). This may have led to increased heat supply to the mantle wedge causing partial melting (e.g., Siegesmund et al., 2023; Oriolo et al., 2021). Ridge subduction-induced orogeny (e.g., Windlay and Xiao, 2018) may explain Ordovician orogenic deformation (e.g., Sardic phase, Stephan et al., 2019), uplift, shortening, and the observed magmatic differentiation to anatectic granitoids with CCG signature, like the Lodnerhütte leucocratic orthogneiss sample LK17-3 (450 Ma). Ridge subduction effects are sensitive to the angle between ridge and trench and to relative and absolute plate motion. Perpendicular to low-angle oblique ridge subduction causes the loss of slab pull as driving force for continued subduction and the end of subduction (e.g., Burkett and Billen, 2009). This is consistent with a Silurian passive-margin setting, as is reported for the Austroalpine (e.g., Schulz et al., 2008; Neubauer et al., 2022).

Siegesmund et al. (2023) located the Ötztal Nappe with other Austroalpine units in a central position of the Ordovician magmatic arc. The position of the Penninic units and the External Massives was more towards the forearc, and the South Alpine units more towards the back arc, except for the Strona-Ceneri Zone which was close to the subduction interface. Ordovician back-arc basin sediments are also reported for the Austroalpine in the Northern Greywacke Zone (Nievoll et al., 2022). An Ordovician and post-Ordovician terrane configuration for intra-Alpine terranes has been proposed (e.g., Frisch and Neubauer, 1989; Ratschbacher and Frisch, 1993; Siegesmund et al., 2021; Neubauer et al., 2022) but is not yet well-constrained for the subunits of the Ötztal Nappe, like the Ötztal Complex s. str., the Texel Complex, the Schneeberg Frame Zone, and the Schneeberg Complex (Klug and Froitzheim, 2021). To keep things simple, we do not include this terrane subdivision in our tectonic model.

9.4. Tectonic model

In Figure 12, we outline a tectonic model for two timesteps of 470 Ma and 450 Ma suggesting a speculative scenario for the magmatic differentiation trend of the Ötztal Nappe/Texel area. The Ordovician active margin of Gondwana was dominated by the preceding accretion of Neo-Proterozoic and Cambrian sediments to the cratonic mainland and the Cadomian magmatic arc. The coexistence of Cadomian and Ordovician magmatic rocks in other Austroalpine units (e.g., Silvretta, Schladming, Northern Defereggen) and in the Central Ötztal Metabasite Zone may be explained by the tectonic incorporation of fragments of the Cadomian arc or even the cratonic mainland into the accretionary complex or by proximity to the mainland. The precursor to the Ordovician magmatic peak may be flat slab subduction with reduced magmatism. As in previous models (e.g., von Raumer et al., 2002; Schulz et al., 2008), the onset of arc magmatism at ca. 470–480 Ma can be explained by an approaching MOR on the lower plate inducing slab steepening and/or slab rollback. The subduction of the MOR leads to a slab window, loss of slab pull, compressional orogeny, uplift and anatectic melting with peraluminous CCG magmatism.

10. Conclusion

In the southeastern Ötztal Nappe and the adjacent Marlengo Slice, orthogneisses yield Ordovician magmatic protolith ages by U-Pb zircon LA-ICPMS dating. The ages trace a differentiation trend from a ~470 Ma old metaluminous granitoid with a geochemical magmatic arc signature, over 450–452 Ma old peraluminous granitoids with an arc to continent-collision signature, to a ~447 Ma old leucocratic granitoid with a collisional to post-orogenic signature. Metaluminous to peraluminous geochemistry and a high abundance of inherited zircon cores show a major sedimentary melt source. The zircon cores of the melt-source sediments exhibit a detrital source in the East-African-Arabian Zircon Province (Stephan et al., 2018) on the northern margin of Gondwana, including a source of late Neoproterozoic Cadomian zircons. The Texel Ordovician granitoid magmatism is probably related to a mid ocean ridge subduction under the active margin of Northern Gondwana dominated by sediment accretion.

Acknowledgements

This work was supported by Deutsche Forschungsgemeinschaft (Grant no. 365184787). We thank Markus Lagos for technical support during laser ablation measurements. The authors are very thankful for the constructive remarks of two anonymous reviewers and for the editorial handling of Walter Kurz.

Supplementary material Tables S1–S6:

Results and details of RFA, EPMA and LA-ICPMS measurements.

References

Autonomous Province Bolzano - South Tyrol, 2024. GeoBrowser. https://maps.civis.bz.it.

Agrawal S., 1995. Discrimination between late-orogenic, post-orogenic, and anorogenic granites by major element compositions. The Journal of Geology, 103/5, 529–537. https://doi.org/10.1086/629774

Avanzini M., Bargossi G., Borsato A., Castiglioni G., Cucato M., Morelli C., Prosser G., Sapelza A., 2007. Erläuterungen zur Geologischen Karte von Italien im Maßstab 1: 50 000 Blatt 026 von Eppan. Servizio Geologico d'Italia.

Bargossi G.M., Bove G., Cucato M., Gregnanini A., Morelli C., Moretti A., Poli S., Zanchetta S., Zanchi A., 2010. Erläuterungen zur geologischen Karte von Italien im Maßstab 1: 50 000 Blatt 013 Meran. CARG. ISPRA, Istituto Superiore per la Protezione e la Ricerca Ambientale. Roma.

Barker F., Farmer G.L., Ayuso R.A., Plafker G., Lull J.S., 1992. The 50 Ma granodiorite of the Eastern Gulf of Alaska: melting in an accretionary prism in the forearc. Journal of Geophysical Research, 97(B5), 6757–6778. https://doi.org/10.1029/92JB00257

Bernhard F., Klötzli U.S., Thöni M., Hoinkes G., 1996. Age, origin and geodynamic significance of a polymetamorphic felsic intrusion in the Ötztal Crystalline Basement, Tirol, Austria. Mineralogy and Petrology, 58/3–4, 171–196. https://doi.org/10.1007/BF01172095

Brandner R., 1980. Geologische Übersichtskarte von Tirol (1:300 000) & Tektonik (1:600 000). In Amt der Tiroler Landesregierung (ed.): Tirol Atlas. Universitäts Verlag Wagner, Innsbruck.

Brocher T.M., Fuis G.S., Fisher M.A., Plafker G., Moses M.J., Taber J.J., Christensen N.I., 1994. Mapping the megathrust beneath the northern Gulf of Alaska using wide-angle seismic data. Journal of Geophysical Research: Solid Earth, 99/B6, 11663–11685. https://doi.org/10.1029/94JB00111

Burkett E.R., Billen M.I., 2009. Dynamics and implications of slab detachment due to ridge-trench collision. Journal of Geophysical Research: Solid Earth, 114/B12. https://doi.org/10.1029/2009JB006402

Cawood P.A., Hawkesworth C.J., Dhuime B., 2012. Detrital zircon record and tectonic setting. Geology, 40/10, 875–878. https://doi.org/10.1130/G32945.1

Chappell B.W., White A.J.R., 1992. I-and S-type granites in the Lachlan Fold Belt. Earth and Environmental Science Transactions of the Royal Society of Edinburgh, 83/1–2, 1–26. https://doi.org/10.1017/S0263593300007720

Chappell B.W., White A.J., 2001. Two contrasting granite types: 25 years later. Australian journal of earth sciences, 48/4, 489–499. https://doi.org/10.1046/j.1440-0952.2001.00882.x

Chew D.M., Petrus J.A., Kamber B.S., 2014. U–Pb LA–ICPMS dating using accessory mineral standards with variable common Pb. Chemical Geology, 363, 185–199. https://doi.org/10.1016/j.chemgeo.2013.11.006

Corfu F., Hanchar J.M., Hoskin P.W.O., 2003. Atlas of Zircon Textures. Reviews in Mineralogy and Geochemistry, 53/1, 469–500. https://doi.org/10.2113/0530469

Debon F., Le Fort P., 1988. A cationic classification of common plutonic rocks and their magmatic associations: principles, method, applications. Bulletin de Minéralogie, 111/5, 493–510. https://doi.org/10.3406/bulmi.1988.8096

Finger F., Riegler G., 2023. The role of the proto-Alpine Cenerian Orogen in the Avalonian-Cadomian belt. Austrian Journal of Earth Sciences, 116/71, 109–115. https://doi.org/10.17738/ajes.2023.0005

Frisch W., Neubauer F., 1989. Pre-Alpine terranes and tectonic zoning in the eastern Alps. Geological Society of America, 230, 91–100. https://doi.org/10.1130/SPE230-p91

Froitzheim N., Conti P.T., Van Daalen M., 1997. Late Cretaceous, synorogenic, low-angle normal faulting along the Schlinig fault (Switzerland, Italy, Austria) and its significance for the tectonics of the Eastern Alps. Tectonophysics, 280/3–4, 267–293. https://doi.org/10.1016/S0040-1951(97)00037-1

GeoSphere Austria, 2024. Multithematische geologische Karte von Österreich 1:1 000 000. online: https://www.geologie.ac.at/services/webapplikationen/multithematische-geologische-karte. GeoSphere Austria - Bundesanstalt für Geologie, Geophysik, Klimatologie und Meteorologie, Wien.

Gregnanin A., Sassi F.P., 1969. Magmatismo, feldspatizzazione e metamorfismo nel complesso gneissico-migmatico di Parcines (Alto Adige). Museo Tridentino di scienze naturali, 18, 57–131.

Habler G., Thöni M., Solva H., 2006. Tracing the high-pressure stage in the polymetamorphic Texel Complex Austroalpine basement unit, Eastern Alps P-T-t-d constraints. Mineralogy and Petrology, 88, 269–296. https://doi.org/10.1007/s00710-006-0143-7

Habler G., Thöni M., Grasemann B., 2009. Cretaceous metamorphism in the Austroalpine Matsch Unit (Eastern Alps): the interrelation between deformation and chemical equilibration processes. Mineralogy and Petrology, 97, 149–171. https://doi.org/10.1007/s00710-009-0094-x

Hauser C., 1992. Geologische Karte der Republik Österreich 1: 50 000 – 117 Zirl. Geologische Bundesanstalt, Wien.

Hammer W., 1911. Die Schichtfolge und der Bau des Jaggl im oberen Vintschgau. Jahrbuch der Kaiserlich Königlichen Geologischen Reichsanstalt. Wien, 61, 1–40.

Hammer, W., 1926. Note illustrative della carta geologica delle Tre Venezie: foglio Passo di Resia. Società cooperativa tipografica.

Hammer, W., 1923. Geologische Spezialkarte der Republik Österreich – Nauders - Maßstab 1:75 000. Geologische Bundesanstalt, Wien.

Hammer, W., 1929. Geologische Spezialkarte der Republik Österreich – Ötzthal – Maßstab 1:75 000. Geologische Bundesanstalt, Wien.

Hoinkes G., Thöni M., 1993. Evolution of the Ötztal-Stubai, Scarl-Campo and Ulten basement units. In: Raumer J.F., Neubauer F. (eds.), Pre-Mesozoic geology in the Alps. Springer Berlin Heidelberg, 485–494. https://doi.org/10.1007/978-3-642-84640-3_29

Institut für Geologie, Universität Bern and Bundesamt für Wasser und Geologie, 2005. Geologische Karte der Schweiz, 1: 50 000. Institut für Geologie, Universität Bern & Bundesamt für Wasser und Geologie, Switzerland.

ISPRA (Istituto Superiore per la Protezione e la Ricerca Ambientale, Dipartimento per il servicio geologico d'Italia (1925) Carta Geologica delle Tre Venezie. In: Foglio 2–3 Passo di Resiá. Carta Geologica d'Italia Scala 1:100 000. ISPRA, Roma.

ISPRA (Istituto Superiore per la Protezione e la Ricerca Ambientale, Dipartimento per il servicio geologico d'Italia (1951) Carta Geologica delle Tre Venezie. In: Foglio 9 Monte Cevedale. Carta Geologica d'Italia Scala 1:100 000. ISPRA, Roma.

ISPRA (Istituto Superiore per la Protezione e la Ricerca Ambientale, Dipartimento per il servicio geologico d'Italia (1957) Carta Geologica delle Tre Venezie. In: Foglio 10 Bolzano. Carta Geologica d'Italia Scala 1:100 000. ISPRA, Roma.

ISPRA (Istituto Superiore per la Protezione e la Ricerca Ambientale, Dipartimento per il servicio geologico d'Italia (1970) Carta Geologica d'Italia Scala. Foglio 4 Meran. In: Carta Geologica d'Italia Scala 1:100 000. ISPRA, Roma.

ISPRA (Istituto Superiore per la Protezione e la Ricerca Ambientale, Dipartimento per il servicio geologico d'Italia (2010) Carta Geologica d'Italia Scala. Foglio 13 Meran. In: Carta Geologica d'Italia Scala 1:50 000. ISPRA, Roma. https://doi.org/10.15161/oar.it/211569

ISPRA (Istituto Superiore per la Protezione e la Ricerca Ambientale, Dipartimento per il servicio geologico d'Italia (2023) Carta Geologica d'Italia Scala. Foglio 6 San Leonardo in Passiria. In: Carta Geologica d'Italia Scala 1:50 000. ISPRA, Roma. https://doi.org/10.15161/oar.it/211561

Janák M., Froitzheim N., Lupták B., Vrabec M., Ravna E.J.K., 2004. First evidence for ultrahigh-pressure metamorphism of eclogites in Pohorje, Slovenia: Tracing deep continental subduction in the Eastern Alps. Tectonics, 23/5, 1–10. https://doi.org/10.1029/2004TC001641

Johannsen A., 1931. A Descriptive Petrography of the Igneous Rocks, Volume I. (88–92). University of Chicago Press, Chicago.

Klötzli E., Teper E., Hörfarter C., 2008. Upper Ordovician basic magmatism in the Austroalpine Realm. Journal of Alpine Geology, 49, 1–127.

Klötzli-Chowanetz E., Klötzli U., Koller F., 1997. Lower Ordovician migmatisation in the Ötztal crystalline basement (Eastern Alps, Austria): linking U-Pb and Pb-Pb dating with zircon morphology. Schweizerische mineralogische und petrographische Mitteilungen, 77, 315–324.

Klug L., 2016. Deformation und Metamorphose im Saltauser Tal (Texelgruppe, Südtirol), Teil 1. University of Bonn, Master thesis.

Klug L., Froitzheim N., 2021. Reuniting the Ötztal Nappe: the tectonic evolution of the Schneeberg Complex. International Journal of Earth Sciences, 1–18. https://doi.org/10.1007/s00531-021-02127-4

Konzett J., Miller C., Armstrong R., Thöni M., 2005. Metamorphic Evolution of Iron-rich Mafic Cumulates from the Ötztal–Stubai Crystalline Complex, Eastern Alps, Austria. Journal of Petrology, 46/4, 717–747. https://doi.org/10.1093/petrology/egh095

Kreuss O., 2011. Geologische Karte Geofast Blatt 145 – Imst. Geologische Bundesanstalt, Wien.

Kreuss O., 2012. Geologische Karte Geofast Blatt 173 – Sölden. Geologische Bundesanstalt, Wien.

Ludwig K. R., 2012. Isoplot 3.75. A geochronological toolkit for Microsoft Excel. Berkeley Geochronology Center, Special Publications, 5, 1–75.

Ludwig K.R., Mundil R., 2002. Extracting reliable U-Pb ages and errors from complex populations of zircons from Phanerozoic tuffs. Geochimica et Cosmochimica Acta, 66(Supplement 1), 463.

Maniar P.D., Piccoli M.P., 1989. Tectonic discrimination of granitoids. Geological Society of American Bulletin, 101, 635–643. https://doi.org/10.1130/0016-7606(1989)101%3C0635:TDOG%3E2.3.CO;2

Meinhold G., Morton A.C., Fanning C.M., Howard J.P., Phillips R.J., Strogen D., Whitham A.G., 2014. Insights into crust formation and recycling in North Africa from combined U-Pb, Lu-Hf and O isotope data of detrital zircons from Devonian sandstone of southern Libya. Geological Society, London, Special Publications, 386/1, 281–292. https://doi.org/10.1144/SP386.1

Miladinova I., Froitzheim N., Nagel T.J., Janak M., Fonseca R.O., Sprung P., Münker C., 2022. Constraining the process of intracontinental subduction in the Austroalpine Nappes: Implications from petrology and Lu-Hf geochronology of eclogites. Journal of Metamorphic Geology, 40/3, 423–456. https://doi.org/10.1111/jmg.12634

Miller C., Thöni M., 1995. Origin of eclogites from the Austroalpine Ötztal basement (Tirol, Austria): geochemistry and Sm-Nd vs. Rb-Sr isotope systematics. Chemical Geology, 122/1–4, 199–225. https://doi.org/10.1016/0009-2541(95)00033-I

Mogessie A., Purtscheller F., Tessadri R., 1985. Geochemistry of amphibolites from the Ötztal-Stubai Complex (Northern Tyrol, Austria). Chemical Geology, 51. 103–113. https://doi.org/10.1016/0009-2541(85)90090-7

Montemagni C., Zanchetta S., Rocca M., Villa I.M., Morelli C., Mair V., Zanchi A., 2023. Kinematics and time-resolved evolution of the main thrust-sense shear zone in the Eo-Alpine orogenic wedge (the Vinschgau Shear Zone, eastern Alps). Solid Earth, 14/5, 551–570. https://doi.org/10.5194/se-14-551-2023

Moser M., 2016a. Geologische Karte Geofast Blatt 116 - Telfs. Geologische Bundesanstalt, Wien.

Moser M., 2016b. Geologische Karte Geofast Blatt 172 - Weißkugel. Geologische Bundesanstalt, Wien.

Müller W., Prosser G., Mancktelow N.S., Villa I.M., Kelley S.P., Viola G., Oberli F., 2001. Geochronological constraints on the evolution of the Periadriatic Fault System (Alps). International Journal of Earth Sciences, 90, 623–653. https://doi.org/10.1007/s005310000187

Neubauer F., Liu Y., Dong Y., Chang R., Genser J., Yuan S., 2022. Pre-Alpine tectonic evolution of the Eastern Alps: from prototethys to paleotethys. Earth-Science Reviews, 226, 103923. https://doi.org/10.1016/j.earscirev.2022.103923

Nievoll J., Fritz H., Gallhofer D., Hauzenberger C., Pfatschbacher M., Gritsch B., 2022. From shallow into deep sea: Sedimentary facies and U-Pb zircon ages in the early Paleozoic Noric Group at Veitsch (Eastern Greywacke Zone, Austria). Austrian Journal of Earth Sciences, 115/1, 41–73. https://doi.org/10.17738/ajes.2022.0003

Nilius N. P., Froitzheim N., Nagel T.J., Tomaschek F., Heuser A., 2016. The Schwarzhorn Amphibolite (Eastern Rätikon, Austria): an Early Cambrian intrusion in the Lower Austroalpine basement. Geologica Carpathica, 67/2, 121–132. https://doi.org/10.1515/geoca-2016-0008

Oriolo S., Schulz B., Geuna S., González P.D., Otamendi J.E., Sláma J., Druguet E., Siegesmund S., 2021. Early Paleozoic accretionary orogens along the Western Gondwana margin. Geoscience Frontiers, 12/1, 109–130. https://doi.org/10.1016/j.gsf.2020.07.001

Paton C., Hellstrom J., Paul B., Woodhead J., Hergt J., 2011. Iolite: Freeware for the visualisation and processing of mass spectrometric data. Journal of Analytical Atomic Spectrometry, 26/12, 2508–2518. https://doi.org/10.1039/C1JA10172B

Pavlik W., Moser M., 2018. Geologische Karte Geofast Blatt 171 - Nauders. Geologische Bundesanstalt, Wien.

Pearce J.A., Harris N.B., Tindle A.G., 1984. Trace element discrimination diagrams for the tectonic interpretation of granitic rocks. Journal of petrology, 25/4, 956–983. https://doi.org/10.1093/petrology/25.4.956

Petrus J.A., Kamber B.S., 2012. VizualAge: A novel approach to laser ablation ICP-MS U-Pb geochronology data reduction. Geostandards and Geoanalytical Research, 36/3, 247–270. https://doi.org/10.1111/j.1751-908X.2012.00158.x

Plafker G., Moore J. C. Winkler G.R., 1994. Geology of the southern Alaska margin. In: Plafker G., Berg H. (eds.), The Geology of North Amerika, Vol. G-1: The geology of Alaska. Geological Society of Amerika, Boulder, Colorado, 389–449. https://doi.org/10.1130/DNAG-GNA-G1.389

Pohl F., Froitzheim N., Obermüller G., Tomaschek F., Schröder O., Nagel T.J., Sciunnach D., Heuser A., 2018. Kinematics and age of syn-intrusive detachment faulting in the Southern Alps: Evidence for Early Permian crustal extension and implications for the Pangea A versus B Controversy. Tectonics, 37/10, 3668–3689. https://doi.org/10.1029/2018TC004974

Pomella H., Stipp M., Fügenschuh B., 2012. Thermochronological record of thrusting and strike-slip faulting along the Giudicarie fault system (Alps, Northern Italy). Tectonophysics, 579, 118–130. https://doi.org/10.1016/j.tecto.2012.04.015

Pomella H., Flöss D., Speckbacher R., Tropper P., Fügenschuh B., 2016. The western end of the Eoalpine High-Pressure Belt (Texel unit, South Tyrol/Italy). Terra Nova, 28/1, 60–69. https://doi.org/10.1111/ter.12191

Raso G., Tropper P., Pomella H., Rammlmair D., 2025. Diabase is petrologists best friend: quantitative P-T constraints on the NW-SE trending Eoalpine metamorphic gradient in the western Austroalpine nappe stack (Ötztal Nappe, Texel Nappe, Silvretta Nappe) using metamorphosed mafic dikes. Austrian Journal of Earth Sciences, 118, 75–94. https://doi.org/10.17738/ajes.2025.0004

Ratschbacher L., Frisch W., 1993. Palinspastic reconstruction of the pre-Triassic basement units in the Alps: the Eastern Alps. In: Raumer J.F., Neubauer F. (eds.), Pre-Mesozoic geology in the Alps. Springer Berlin Heidelberg, 41–51. https://doi.org/10.1007/978-3-642-84640-3_4

Rockenschaub M., Nowotny A., 2009. Geological map sheet 148 Brenner 1:50 000. Geologische Bundesanstallt, Wien.

Rockenschaub M., Nowotny A., 2011. Geological map sheet 175 Sterzing 1:50 000. Geologische Bundesanstalt, Wien.

Rondenay S., Montési L.G., Abers G.A., 2010. New geophysical insight into the origin of the Denali volcanic gap. Geophysical Journal International, 182/2, 613–630. https://doi.org/10.1111/j.1365-246X.2010.04659.x

Salze M., Martinod J., Guillaume B., Kermarrec J.J., Ghiglione M.C., Sue C., 2018. Trench-parallel spreading ridge subduction and its consequences for the geological evolution of the overriding plate: Insights from analogue models and comparison with the Neogene subduction beneath Patagonia. Tectonophysics, 737, 27–39. https://doi.org/10.1016/j.tecto.2018.04.018

Schindlmayr A., 1999. Granitoids and Plutonic Evolution of the Ötztal-Stubai Massif – A Key for Understanding the Early Palaeozoic History of the Austroalpine Crystalline Basement on the Western Eastern Alps. University of Salzburg, Dissertation.

Schmid S.M., Haas R., 1989. Transition from near-surface thrusting to Intrabasement Decollement, Schlinig Thrust, eastern Alps. Tectonics, 8/4, 697–718. https://doi.org/10.1029/TC008i004p00697

Schneider T., 2013. Petrologie und Strukturgeologie eines Nb-Ta-Sn-UP-Be-führenden Pegmatits im Austroalpinen Texel-Komplex. University of Innsbruck, Master thesis.

Schulz B., Steenken A., Siegesmund S., 2008. Geodynamic evolution of an Alpine terrane - the Austroalpine basement to the south of the Tauern window as a part of the Adriatic Plate (eastern Alps). Geological Society, London, Special Publications, 298/1, 5–44. https://doi.org/10.1144/SP298.2

Schuster R., 2003. Das eo-Alpine Ereignis in den Ostalpen: Plattentektonische Situation und interne Struktur des Ostalpinen Kristallins. Arbeitstagung der Geologischen Bundesanstalt Blatt, 148, 141–159.

Siegesmund S., Oriolo S., Schulz B., Heinrichs T., Basei M.A.S., Lammerer B., 2021. The birth of the Alps: Ediacaran to Paleozoic accretionary processes and crustal growth along the northern Gondwana margin. International Journal of Earth Sciences, 110/4, 1321–1348. https://doi.org/10.1007/s00531-021-02019-7

Siegesmund S., Oriolo S., Broge A., Hueck M., Lammerer B., Basei M.A., Schulz B., 2023. Cadomian to Cenerian accretionary orogenic processes in the Alpine basement: the detrital zircon archive. International Journal of Earth Sciences, 112/4, 1157–1174. https://doi.org/10.1007/s00531-023-02305-6

Sláma J., Košler J., Condon D.J., Crowley J.L., Gerdes A., Hanchar J.M., et al., 2008. Plešovice zircon - A new natural reference material for U-Pb and Hf isotopic microanalysis. Chemical Geology, 249, 1–35. https://doi.org/10.1016/j.chemgeo.2007.11.005

Söllner V.F., Hansen B.T., 1987. „Pan-afrikanisches" und „kaledonisches"

Ereignis im Ötztal-Kristallin der Ostalpen: Rb-Sr- und U-Pb-Altersbestimmungen an Migmatiten und Metamorphiten. Jahrbuch der Geologischen Bundesanstalt, 130/4, 529–569.

Sölva H., Thoni M., Grasemann B., Linner M., 2001. Emplacement of Eoalpine high-pressure rocks in the Austroalpine Ötztal complex, Texel group, Italy/Austria. Geodinamica Acta, 14, 345–360. https://doi.org/10.1016/S0985-3111(01)01072-5

Spiess R., Cesare B., Mazzoli C., Sassi R., Sassi F.P., 2010. The crystalline basement of the Adria microplate in the eastern Alps: a review of the palaeostructural evolution from the Neoproterozoic to the Cenozoic. Rendiconti Lincei, 21, 31–50. https://doi.org/10.1007/s12210-010-0100-6

Stampfli G.M., 2000. Tethyan oceans. Geological society, London, special publications, 173/1, 1–23. https://doi.org/10.1144/GSL.SP.2000.173.01.01

Stampfli G.M., Hochard C., Vérard C., Wilhem C., 2013. The formation of Pangea. Tectonophysics, 593, 1–19. https://doi.org/10.1016/j.tecto.2013.02.037

Stephan T., Kroner U.W.E., Romer R.L., 2019. The pre-orogenic detrital zircon record of the Peri-Gondwanan crust. Geological Magazine, 156/2, 281–307. https://doi.org/10.1017/S0016756818000031

Stephan T., Kroner U., Romer R.L., Rösel D., 2019. From a bipartite Gondwanan shelf to an arcuate Variscan belt: the early Paleozoic evolution of northern Peri-Gondwana. Earth-Science Reviews, 192, 491–512. https://doi.org/10.1016/j.earscirev.2019.03.012

Thöni M., 1973. Ein neues Sedimentvorkommen nahe dem Westrand des Ötztaler Altkristallins und einige Bemerkungen zur Deutung der Permotrias des Jaggl als Fenster. Verh. Geol. Bundesanst. Wien, 1973, 235–712.

Thöni M., 1981. Degree and evolution of the Alpine metamorphism in the Austroalpine unit W of the Hohe Tauern in the light of K/Ar and Rb/Sr age determinations on micas. Jahrbuch der geologischen Bundesanstalt, 124/1, 111–174.

Tropper P., Tribus M., Pomella H., Habler G., 2023. The metabasites from the Texel Unit (Austroalpine nappe stack): markers of Cretaceous intracontinental subduction and subsequent collision. Austrian Journal of Earth Sciences, 116, 165–179. https://doi.org/10.17738/ajes.2023.0010

van Gool J., 1985. Structural Geology of the Southwestern Ötztal Alps Between the Weisskugel and the Reschensee. University of Utrecht. Diploma thesis.

Vermeesch P., 2012. On the visualisation of detrital age distributions. Chemical Geology, 312, 190–194. https://doi.org/10.1016/j.chemgeo.2012.04.021

Vermeesch P., 2018. IsoplotR: A free and open toolbox for geochronology. Geoscience Frontiers, 9(5), 1479–1493. https://doi.org/10.1016/j.gsf.2018.04.001

Vielzeuf D., Holloway J.R., 1988. Experimental determination of the fluid-absent melting relations in the pelitic system: consequences for crustal differentiation. Contributions to Mineralogy and Petrology, 98, 257–276. https://doi.org/10.1007/BF00375178

Villaseca C., Barbero L., Herreros V., 1998. A re-examination of the typology of peraluminous granite types in intracontinental orogenic belts. Earth and Environmental Science Transactions of The Royal Society of Edinburgh, 89/2, 113–119. https://doi.org/10.1017/S0263593300007045

Von Raumer J.F., 1998. The Palaeozoic evolution in the Alps: from Gondwana to Pangea. Geologische Rundschau, 87, 407–435. https://doi.org/10.1007/s005310050219

Von Raumer J., Stampfli G., Borel G., Bussy F., 2002. Organization of pre-Variscan basement areas at the north-Gondwanan margin. International Journal of Earth Sciences, 91, 35–52. https://doi.org/10.1007/s005310100200

Von Raumer J.F., Bussy F., Schaltegger U., Schulz B., Stampfli G.M., 2013. Pre-Mesozoic Alpine basements - their place in the European Paleozoic framework. Bulletin, 125/1–2, 89–108. https://doi.org/10.1130/B30654.1

von Raumer J.F., Stampfli G.M., 2008. The birth of the Rheic Ocean - Early Palaeozoic subsidence patterns and subsequent tectonic plate scenarios. Tectonophysics, 461/1–4, 9–20. https://doi.org/10.1016/j.tecto.2008.04.012

Viola G., Mancktelow N.S., Seward D., 2001. Late Oligocene-Neogene evolution of Europe-Adria collision: New structural and geochronological evidence from the Giudicarie fault system (Italian Eastern Alps). Tectonics, 20/6, 999–1020. https://doi.org/10.1029/2001TC900021

Whalen J.B., Currie K.L., Chappell B. W., 1987. A-type granites: geochemical characteristics, discrimination and petrogenesis. Contributions to mineralogy and petrology, 95, 407–419. https://doi.org/10.1007/BF00402202

Windley B.F., Xiao W., 2018. Ridge subduction and slab windows in the Central Asian Orogenic Belt: Tectonic implications for the evolution of an accretionary orogen. Gondwana Research, 61, 73–87. https://doi.org/10.1016/j.gr.2018.05.003

Zanchetta S., Poli, S., Rubatto, D., Zanchi, A., Bove, G., 2013. Evidence for deep subduction of Austroalpine crust Texel Complex, NE Italy. Rendiconti Lincei, 24, 163–176. https://doi.org/10.1007/s12210-013-0239-z

Zantedeschi C., 1991. Geocronologia Rb–Sr sugli gneiss granitoidi del Complesso di Parcines (Alto Adige Occidentale). Memorie della Società Geologica Italiana, 43, 319–329.

Zurbriggen R., 2015. Ordovician orogeny in the Alps: a reappraisal. International Journal of Earth Sciences, 104/2, 335–350. https://doi.org/10.1007/s00531-014-1090-x

Zurbriggen R., 2017. The Cenerian orogeny (early Paleozoic) from the perspective of the Alpine region. International Journal of Earth Sciences, 106/2, 517–529. https://doi.org/10.1007/s00531-016-1438-5

Zurbriggen R., 2020. Banded amphibolites in the Alps: a new interpretation in relation to early Paleozoic peraluminous magmatism. Swiss Journal of Geosciences, 113/1, 1–24. https://doi.org/10.1186/s00015-020-00362-6

Received: 28.10.2024
Accepted: 26.2.2025
Editorial Handling: Walter Kurz